

Dielectric Properties of Semicrystalline Polychlorotrifluoroethylene

Arnold H. Scott, Donald J. Scheiber, Alexander J. Curtis, John I. Lauritzen, Jr.,
and John D. Hoffman

(April 2, 1962)

The dielectric properties of polychlorotrifluoroethylene ($T_m=224^\circ\text{C}$, $T_g=52^\circ\text{C}$) have been measured at temperatures between -50 and $+250^\circ\text{C}$, and at frequencies between 0.1 c/s and 8.6 kMc/s. Specimens of known crystallinities, ranging from $\chi=0.80$ to $\chi=0.00$ (pure liquid) were studied. Comprehensive tables of data are presented. The experimental techniques employed to measure the dielectric properties over these wide ranges of temperature, frequency, physical state, and sample type (disks, cylinders, and thin films), are discussed. The operation and calibration of the specimen holder, bridges, resonant circuits, and waveguide apparatus used are discussed in detail.

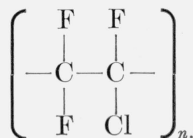
When the dielectric loss index, ϵ'' , at 1 c/s is plotted as a function of temperature for a highly crystalline specimen ($\chi=0.80$), where the crystallinity consists largely of lamellar spherulites, three distinct loss peaks are readily apparent. These peaks occur at about -40°C (low-temperature process), 95°C (intermediate-temperature process), and 150°C (high-temperature process). The dielectric data are compared with the mechanical loss data obtained at 1 c/s by McCrum. Mechanical loss peaks at temperatures virtually identical to those in the ϵ'' versus T plot are found.

The *high-temperature* process is attributed to the presence of well-formed chain-folded lamellar spherulites. Some evidence points to the surfaces of the lamellae as the site of the loss mechanism. The high-temperature loss peak does not appear in resolved form in non-spherulitic specimens even when the crystallinity is high. The *intermediate-temperature* process originates in the normal supercooled amorphous phase, and is due to the complex dipole relaxation effects involving motions of large numbers of polymer chain segments that are associated with the onset of the glass transition at $T_g=52^\circ\text{C}$. As determined by $\bar{V}-T$ data, the glass transition temperature at $T_g=52^\circ\text{C}$ that is associated with this relaxation effect does not shift appreciably with increasing crystallinity. The *low-temperature* dielectric loss process, which is active far below T_g , originates principally in the supercooled amorphous regions, and evidently corresponds to a fairly simple motion involving a small number of chain segments. This process tends to exhibit anomalous behavior in highly crystalline specimens, particularly at low temperatures.

A large dipolar contribution of the crystals to the static dielectric constant was observed. This contribution increased with increasing temperature, and corresponded to a very rapid dipole reorientation process ($\tau\sim 10^{-11}$ sec at 23°C).

1. Introduction

Polychlorotrifluoroethylene, abbreviated here as PCTFE, has the chemical repeat unit



The molecular asymmetry of the repeat unit gives rise to a permanent dipole moment that subtends a right angle to the carbon chain axis.

Our original interest in investigating the dielectric behavior of this substance stemmed in large part from the fact that the polymer molecule possesses no side groups capable of independent orientation, such as complicate the investigation of certain other polymer systems. In PCTFE, one can be quite certain that any dielectric relaxation effects that are observed, whether originating in the crystalline or

amorphous components, are to be attributed to motions involving portions of the polymer chain backbone.

The dielectric properties of PCTFE were investigated over a limited range of temperature and frequency by Reynolds, Thomas, Sharbaugh, and Fuoss [1]¹ in 1951. It was clearly established by them that the dielectric properties of low molecular weight PCTFE waxes were strongly affected when crystallization took place. A high molecular weight specimen was also studied, but the effect of changing degree of crystallinity was not investigated. Hartshorn, Parry, and Rushton [2], and Mikhailov and Sazhin [3], studied high molecular weight PCTFE⁹ and gave more extensive information on its dielectric properties. In these later studies, samples of varying but unknown degrees of crystallinity were investigated, so that only a qualitative connection could be established between degree of crystallinity and dielectric properties.

¹ Figures in brackets indicate the literature references at the end of this paper.

Hoffman and Weeks [4] have demonstrated a means whereby the degree of crystallinity of PCTFE over a wide range of temperature can be simply and accurately determined by measurements of the specific volume. This facilitates an attempt at a quantitative analysis of the dielectric data in terms of the degree of crystallinity.

The present investigation was undertaken to provide accurate dielectric data upon samples of known thermal history and degree of crystallinity over a wide temperature range (-50 to $+250$ °C), and a frequency range (0.1 to almost 10^{10} c/s) much broader than that studied by earlier investigators. From these data, an attempt can then be made to correlate the observed dielectric behavior with the degree of crystallinity and other variables. Special interest attaches to the identification of the contributions of the amorphous and crystalline phases to the dielectric behavior, and to differences in dielectric properties exhibited by specimens of nearly identical crystallinity prepared by different crystallization techniques.

The extension of the frequency range down to 0.1 c/s is made possible by the use of a low-frequency bridge described in detail elsewhere [5]. Nakajima and Saito [6] have reported measurements of the dielectric properties of PCTFE in the frequency range of 0.1 to 10^6 c/s in which a bridge of rather similar capabilities was used.

2. Specimens

2.1. Materials

All specimens used in this investigation were prepared from laboratory samples of Kel-F grade 300 polymer, which was supplied in sheet form by Dr. H. S. Kaufman. The number average molecular weight of the polymer was stated to be approximately 415,000. The equilibrium melting point of the crystals in the polymer is estimated to be 224 ± 1 °C [7]. If the crystals are small, as is the case when they are formed at large or moderate subcooling, the observed melting point of a specimen will be somewhat lower, values ranging from 212 to 218 °C being commonly observed [7]. The normal glass transition in the amorphous component of this semicrystalline polymer is at 52 °C, as determined by the change of slope of volume-temperature curves [4].

2.2. Preparation of Specimens

The specimens employed in this investigation are divided into five categories determined by their degree of crystallinity and thermal history. The determination of the degree of crystallinity, χ , is given in section 2.4. In general, the specimen designations denote the degree of crystallinity of the material.

a. Specimen 0.80

The three specimens described below had degrees of crystallinity near $\chi=0.80$ and similar thermal his-

ories. These specimens are therefore referred to jointly as "specimen 0.80." They were prepared from PCTFE that had been crystallized from the melt according to the procedure of Hoffman and Weeks [4]. The material was heated to 250 °C, which is well above the melting point, and then brought successively to temperatures of 200 and 190 °C, residing one day at each of these temperatures. The material was then maintained at 180 °C for three days, after which it was cooled to room temperature over a period of a few hours. Typical spherulitic crystallization occurs under these conditions. This cloudy-white material was then machined into a disk-shaped specimen, 4.2448 cm in diameter, which was called specimen 0.80A. Dielectric measurements were made upon specimen 0.80A using the Schering bridge and Q -meter described in appendix 6.3. Specimen 0.80B was then prepared from specimen 0.80A by machining the disk down to about 2.54 cm in diameter, the specimen diameter required by the re-entrant cavity described in appendix 7.1. Specimen 0.80B was employed in measurements involving the re-entrant cavity and the low-frequency bridge (0.1 to 200 c/s). The specimens employed in the microwave measurements were prepared by nearly the same procedure, and attained a degree of crystallinity of 78 percent.

The general method of crystallization described above is referred to as "crystallization from the melt" in the text.

The reader is cautioned that the name "specimen 0.80" is not intended to imply that the degree of crystallinity of the specimen always remains at $\chi=0.80$. As is discussed below, the degree of crystallinity of this specimen decreases appreciably when it is heated above about 175 °C.

b. Specimen 0.44

We refer here to two disk-shaped specimens of different diameters which were both 44 percent crystalline. They were prepared from bulk material about 2 mm thick which had been previously heated above the melting point to 250 °C, and then plunged into ice water. Specimen 0.44A was a disk 4.4033 cm in diameter. Specimen 0.44B was prepared by machining specimen 0.44A to a diameter of about 2.54 cm. Specimen 0.44A and 0.44B are jointly referred to as "specimen 0.44." These specimens had a slightly opalescent appearance, but were optically much clearer than specimen 0.80. The above technique is referred to in the text as "quench crystallization."

c. Specimen 0.12

This specimen was 12 percent crystalline. It was prepared from a thin film about 0.15 mm thick which had been pressed from the bulk material, heated to 250 °C, and plunged into ice water. The resultant thin film was optically clear.

In order to study the dielectric properties of nearly amorphous PCTFE at low temperatures, it

is necessary to resort to measuring quenched thin films rather than thick specimens. This is the case because between 120 and 170 °C there exists a temperature region in which extremely rapid crystallization takes place [7], and a thick specimen (say 2 mm thick) cannot be cooled rapidly enough through this region to prevent a significant amount of crystallization. A thin film having a large surface-to-volume ratio may be quenched more rapidly than the bulk material, thus achieving a lower degree of crystallinity. Such a weakly crystalline film will crystallize further if heated above approximately 60 °C.

d. Specimen 0.73

This specimen was prepared by annealing specimen 0.44B (quench crystallized bulk material) at 190 °C for two weeks. This increased the degree of crystallinity to $\chi=0.73$. It is important to note that this specimen was *not* crystallized directly from the melt as was specimen 0.80, but rather from a previously quenched specimen. This was done so that the dielectric properties of specimens with nearly the same high degree of crystallinity, but with crystals nucleated and grown under different conditions, might be compared. This crystallization process is referred to as the "quench→anneal" technique.

e. Specimen 0.0 (Liquid Phase)

By warming a disk specimen above $T_m=224$ °C, a body with no crystallinity ($\chi=0.00$) could be readily obtained. A specimen made in this way was studied up to 250 °C. Then by supercooling, the completely amorphous phase was studied down to about 200 °C. The onset of crystallization prevented measurements below this temperature.² Details of the methods used to obtain dielectric measurements on the liquid specimens, which tended to flow somewhat, are given in appendix 5.3.

Figure 1 shows the temperature dependence of the degree of crystallinity and the specific volume of the various specimens.

All the above mentioned specimens, with the exception of those used for the microwave measurements, and specimen 0.0, were machined or cut into disk shapes with areas and thicknesses determined by methods given below.

2.3. Determination of Dimensions of Disk Specimens

The area A^{23} at 23 °C was calculated from the average of several measurements of the specimen's diameter taken from various points on the circumference. A traveling microscope graduated to 0.0001 cm was employed for this purpose.

The average thickness of the specimen t^{23} at 23 °C was not directly measured but was calculated from

² The rate of crystallization increases as the temperature is lowered below T_m . At 210 °C, the rate of crystallization from the supercooled liquid is altogether negligible, but below about 200 °C, the rate becomes high enough to interfere in the time required to measure ϵ' and ϵ'' .

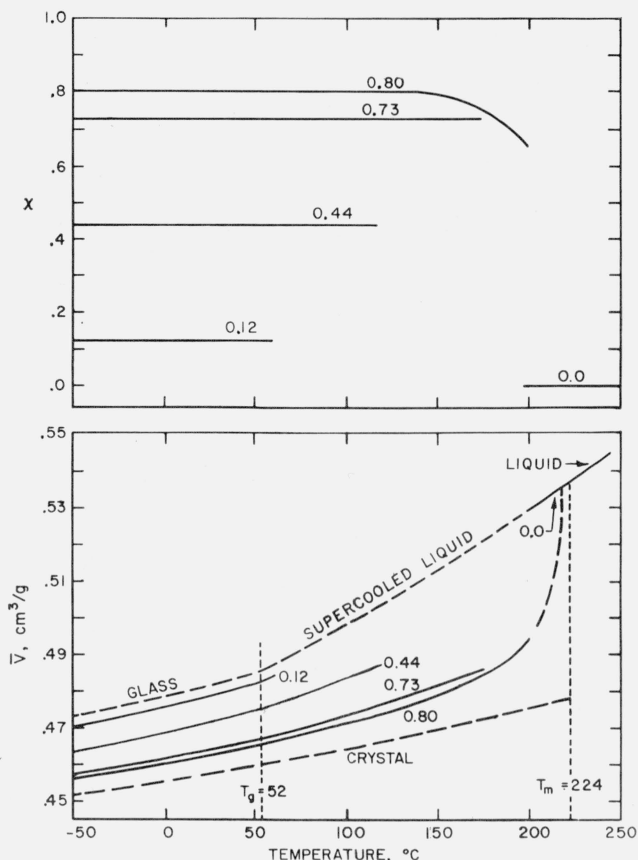


FIGURE 1. Temperature dependence of the degree of crystallinity, χ , and the specific volume, \bar{V} , of the specimens.

the equation

$$t^{23} = \frac{V^{23}}{A^{23}} = \frac{\bar{V}^{23} W_{\text{air}}}{A^{23}}, \quad (1)$$

where \bar{V}^{23} is the specific volume at 23 °C, W_{air} the weight of the specimen in air, and V^{23} is the volume of the specimen at 23 °C. The specific volume employed in eq (1) was measured using the buoyancy technique. The specimen was weighed in air, and then in distilled water³ at 23 °C (W_{water}). Given the density of the water, ρ_{water} , the specific volume was calculated from the equation

$$\bar{V}^{23} = \frac{W_{\text{air}} - W_{\text{water}}}{\rho_{\text{water}} W_{\text{air}}} \quad (2)$$

A discussion of the accuracy of the measurements of A^{23} and t^{23} is given in appendix 5.1.e.

The above method of determining the average thickness of a specimen is distinctly superior to direct measurements using a micrometer, particularly for molded or machined specimens which have

³ Distilled water was selected as a suitable immersion fluid for PCTFE since the density of water is very well known and since the water absorption of PCTFE is unmeasurably small. A small quantity of wetting agent was added to the water to reduce surface tension. This affected the density of the water by no more than 10 ppm.

TABLE 1. Physical characteristics of the disk and thin film specimens

Specimen	Degree of crystallinity χ	Remarks	Specific volume at 23 °C, \bar{V}^{23}	Area, A^{23}	Thickness t^{23}	Vacuum capacitance C_v^{23}
0.80A 0.80B	0.80	Crystallized slowly from melt. Specimen highly spherulitic. Has white cloudy appearance.	$cm^3 g^{-1}$ 0.4625 .4624	cm^2 14.141 5.0523	cm 0.2315 .2309	pf 5.408 1.937
0.44A 0.44B	.44	Quench crystallized. Specimen contains no visible spherulites. Optically rather transparent.	.4711 .4711	15.228 5.0658	.1840 .1832	7.328 2.448
0.73	.73	Crystallized by quench \longrightarrow anneal method. Specimen contains no visible spherulites. Optically fairly transparent.	.4642	5.0561	.1750	2.558
0.12	.12	Prepared by rapid quenching of thin film. Optically transparent.	.4788	20.333	.01464	123.0

the usual slight surface irregularities. (The effect of such surface irregularities upon the dielectric measurements is considered in appendix 5.3.) In measuring a rigid material, a micrometer reads the *maximum* thickness of the material between its faces, and unless the two surfaces are perfect, the desired *average* thickness is not obtained. Using the specific volume method outlined above, the measurement "probe" consists of the liquid which establishes intimate contact with the surface, following its minute irregularities. Furthermore, if the material whose thickness is desired is somewhat soft, use of a micrometer tends to compress the specimen between its faces. Immersion in a liquid subjects the specimen only to very mild and uniform pressures.

The values of A and t at other temperatures are calculable from the change in specific volume with temperature, which has been previously measured [4].

Values of \bar{V}^{23} , A^{23} , t^{23} , and C_v^{23} for the specimens employed are given in table 1. Here C_v^{23} is the equivalent vacuum capacitance of the specimen at 23 °C expressed in pf.⁴ C_v is given by

$$C_v^{23} = \epsilon_0 \frac{A^{23}}{t^{23}}, \quad (3)$$

where ϵ_0 is the electric constant in the mks rationalized system ($\epsilon_0 = 8.854 \times 10^{-12}$ F/m, = 0.08854 pf/cm).

After determining the above physical characteristics, the specimens were given conducting coatings. The planar surfaces of specimens 0.80A, 0.80B, 0.44, and 0.73 were given a conductive coating of evaporated gold, while silver conducting paint (silver 4922, manufactured by E. I. DuPont de Nemours and Co.) was applied to specimen 0.12.

2.4. Determination of χ

The degree of crystallinity of a specimen of PCTFE (defined here as the *mass* fraction crystallized) is at any temperature defined by the equation

$$\chi = \frac{\bar{V}_l - \bar{V}}{\bar{V}_l - \bar{V}_c}, \quad (4)$$

where \bar{V}_l is the specific volume of the pure liquid (or glass), \bar{V}_c is the specific volume of the pure crystal, and \bar{V} the specific volume of the specimen in $cm^3 g^{-1}$.

The values of \bar{V}_l and \bar{V}_c at 23 °C are 0.48175 and 0.45755 respectively [4]. One may then write for the degree of crystallinity at 23 °C

$$\chi = \frac{0.48175 - \bar{V}^{23}}{0.0242}. \quad (5)$$

Using this formula, χ can be simply determined from the value of \bar{V}^{23} .

The value of χ remains constant with temperature as long as those temperature regions in which melting or further crystallization can take place are avoided. In order to avoid further crystallization of specimens 0.44 and 0.12, they were not heated above 118 and 60.6 °C, respectively.

Specimen 0.80, for which dielectric measurements were made up to 200 °C, underwent a significant amount of partial melting between 175 and 200 °C. (This partial melting is actually due to the complete melting out of the smaller crystals in the material.) In this region, the value of χ decreased, but the process was reversible as long as the specimen was brought down in temperature reasonably slowly. The temperature dependence of χ in this region is shown in figure 1. These curves were obtained from earlier work [4]. At 150, 175, and 200 °C, the value of χ for specimen 0.80 is 0.79, 0.75, and 0.65 respectively. In any analysis of the data in terms of χ , the variation of χ in this temperature range should not be neglected.

3. Experimental Results

The reader is referred to the appendix for discussion of the experimental details related to the specimen holder, bridges, Q -meter, re-entrant cavity, and waveguide apparatus employed in making the measurement of the loss index, ϵ'' , and the real part of the relative dielectric constant, ϵ' .

The results of dielectric measurements are presented in both graphical and tabular form. The experimental points are shown on some of the plots to give an indication of the accuracy. From the

⁴ 1 pf = 1 picofarad = 1 $\mu\mu$ f.

TABLE 2. Smoothed dielectric data for specimen 0.80

If $\delta\epsilon'$ and $\delta\epsilon''$ represent the possible error in the values of ϵ' and ϵ'' reported below, then, when $f < 100$ kc/s $\delta\epsilon' = 0.15\%$ and $\delta\epsilon'' = 1\%$. When 100 kc/s $< f \leq 10$ Mc/s then $\delta\epsilon' = 0.5\%$ and $\delta\epsilon'' = 5\%$.

Temperature / Frequency		-50 °C		-35.5 °C		-25 °C		0 °C	
		ϵ'	$\epsilon'' \times 10^4$						
0.1 c/s	2.597	360	2.653	264	2.684	187	2.740	100	
.2	2.582	382	2.641	304	2.674	221	2.734	113	
.5	2.559	389	2.621	355	2.661	279	2.727	139	
1	2.540	378	2.604	391	2.647	326	2.721	160	
2	2.522	355	2.584	415	2.631	370	2.713	189	
5	2.500	312	2.558	423	2.605	421	2.702	239	
10	2.486	279	2.539	410	2.586	449	2.690	298	
20	2.474	243	2.519	380	2.565	457	2.675	364	
50	2.461	198	2.498	326	2.538	426	2.651	445	
100	2.454	167	2.485	282	2.520	382	2.629	488	
200	2.447	145	2.473	240	2.503	335	2.604	511	
500	2.438	126	2.461	190	2.485	269	2.571	487	
1 kc/s	2.433	113	2.454	163	2.474	224	2.548	444	
2	2.428	104	2.446	145	2.464	192	2.529	391	
5	2.423	95	2.438	128	2.455	165	2.507	320	
10	2.418	91	2.433	120	2.448	151	2.495	275	
20	2.415	87	2.427	112	2.441	139	2.485	238	
50	2.410	82	2.422	104	2.434	126	2.472	200	
100	2.407	78	2.417	100	2.428	120	2.464	183	
200	2.404	74	2.413	96	2.424	115	2.456	170	
310	2.402	70	-----	-----	2.420	112	2.451	165	
1 Mc/s	2.397	64	-----	-----	2.412	104	2.441	155	
3.2	2.393	57	-----	-----	2.405	96	2.431	149	
10	2.390	51	-----	-----	2.397	92	2.421	144	

Temperature / Frequency		23 °C		50 °C		75 °C		100 °C	
		ϵ'	$\epsilon'' \times 10^4$						
0.1 c/s	2.772	53	2.798	26	2.832	61	2.862	58	
.2	2.770	60	2.797	26	2.831	56	2.860	58	
.5	2.765	75	2.796	30	2.827	50	2.858	58	
1	2.762	88	2.794	34	2.824	45	2.856	58	
2	2.758	105	2.793	38	2.821	40	2.854	59	
5	2.751	133	2.791	49	2.818	35	2.849	60	
10	2.746	162	2.788	59	2.816	33	2.846	61	
20	2.737	197	2.785	72	2.815	35	2.842	63	
50	2.725	257	2.781	100	2.812	44	2.838	65	
100	2.714	315	2.777	130	2.810	54	2.835	66	
200	2.700	387	2.772	175	2.808	67	2.832	68	
500	2.672	490	2.760	267	2.804	95	2.828	70	
1 kc/s	2.646	549	2.748	348	2.800	131	2.825	76	
2	2.618	572	2.733	445	2.796	188	2.822	90	
5	2.578	536	2.700	581	2.784	294	2.818	117	
10	2.555	477	2.672	640	2.771	413	2.812	166	
20	2.534	413	2.641	650	2.751	544	2.807	244	
50	2.510	335	2.596	595	2.706	683	2.792	404	
100	2.498	292	2.571	535	2.671	745	2.771	561	
200	2.488	263	2.552	479	2.641	754	2.744	744	
310	2.483	248	2.541	442	2.623	716	2.725	803	
1 Mc/s	2.468	229	2.516	363	2.581	586	2.665	830	
3.2	2.454	208	2.493	306	2.547	485	2.602	737	
10	2.440	190	2.475	275	2.515	425	2.552	637	
292	2.402	155	-----	-----	-----	-----	2.470	403	
1 k Mc/s	2.388	155	-----	-----	-----	-----	-----	-----	
3	2.375	165	-----	-----	-----	-----	-----	-----	
8.6	2.360	180	-----	-----	-----	-----	-----	-----	

Temperature / Frequency		125 °C		150 °C		175 °C		200 °C	
		ϵ'	$\epsilon'' \times 10^4$						
0.1 c/s	2.887	58	2.926	80	2.958	102	2.955	532	
.2	2.886	57	2.923	78	2.956	66	2.946	330	
.5	2.883	55	2.918	78	2.955	42	2.942	175	
1	2.881	54	2.915	80	2.955	35	2.941	121	
2	2.879	53	2.913	83	2.954	30	2.940	79	
5	2.877	52	2.910	85	2.953	29	2.940	38	
10	2.874	52	2.908	85	2.952	33	2.939	23	
20	2.871	54	2.905	83	2.950	42	2.939	15	
50	2.868	58	2.900	79	2.948	58	2.939	11	
100	2.863	61	2.896	76	2.945	70	2.938	11	
200	2.861	65	2.892	74	2.942	83	2.938	13	
500	2.858	71	2.888	73	2.937	99	2.937	20	
1 kc/s	2.854	77	2.885	72	2.932	111	2.937	28	
2	2.852	82	2.882	72	2.927	137	2.935	40	
5	2.846	92	2.878	82	2.919	119	2.933	58	
10	2.842	104	2.875	92	2.913	116	2.930	73	
20	2.839	127	2.871	107	2.908	113	2.927	89	
50	2.832	187	2.865	131	2.902	123	2.920	111	
100	2.825	277	2.860	175	2.898	142	2.916	127	
200	2.814	432	2.854	243	2.892	171	2.913	146	
310	2.808	552	2.848	314	2.887	214	2.909	158	
1 Mc/s	2.757	826	2.823	608	2.867	421	2.900	246	
3.2	2.688	920	2.768	821	2.825	793	2.882	518	
10	2.610	873	2.700	1018	2.762	1090	2.849	1013	
292	-----	-----	2.560	852	-----	-----	-----	-----	

TABLE 3. Smoothed dielectric data for specimen 0.44

$\delta\epsilon'$ and $\delta\epsilon''$, the possible error in the values of ϵ' and ϵ'' reported below, are functions of the frequency and temperature. When $T < 50^\circ\text{C}$ and $f \leq 100$ kc/s then $\delta\epsilon' = 0.15\%$ and $\delta\epsilon'' = 1\%$. When $T < 50^\circ\text{C}$ and 100 kc/s $< f \leq 10$ Mc/s then $\delta\epsilon' = 0.5\%$ and $\delta\epsilon'' = 5\%$. When $T > 50^\circ\text{C}$ and $f \leq 100$ kc/s and $\delta\epsilon' = 0.6\%$ and $\delta\epsilon'' = 1.5\%$ and when $T > 50^\circ\text{C}$ and 100 kc/s $< f \leq 10$ Mc/s then $\delta\epsilon' = 1\%$ and $\delta\epsilon'' = 6\%$.

Temperature Frequency	-50 °C		-36 °C		-24.5 °C		+0.5 °C	
	ϵ'	$\epsilon'' \times 10^4$						
0.1 c/s	2.473	274	2.531	253	2.570	240	2.663	186
.2	2.459	289	2.518	278	2.560	264	2.654	203
.5	2.442	295	2.501	305	2.544	297	2.640	234
1	2.428	287	2.486	320	2.529	320	2.628	264
2	2.414	268	2.471	325	2.514	343	2.616	299
5	2.399	238	2.450	321	2.491	358	2.598	352
10	2.390	215	2.435	309	2.474	369	2.582	393
20	2.382	191	2.421	288	2.456	369	2.563	435
50	2.372	160	2.404	248	2.434	336	2.535	475
100	2.367	137	2.393	217	2.419	300	2.513	485
200	2.361	117	2.384	189	2.407	265	2.489	475
500	2.355	98	2.373	154	2.392	219	2.461	439
1 kc/s	2.351	86	2.367	130	2.384	190	2.442	400
2	2.347	75	2.361	110	2.376	165	2.426	356
5	2.344	65	2.354	93	2.368	134	2.406	292
10	2.341	61	2.351	85	2.363	115	2.395	247
20	2.338	58	2.348	78	2.358	100	2.384	210
50	2.335	54	2.344	73	2.352	87	2.373	170
100	2.333	51	2.340	69	2.348	81	2.366	147
200	2.331	48	2.338	66	2.344	79	2.361	127
310	2.330	46					2.357	118
1 Mc/s	2.326	41					2.349	95
3.2	2.324	36					2.340	82
10	2.321	30					2.334	73

Temperature Frequency	23 °C		50 °C		75 °C		100 °C		118 °C	
	ϵ'	$\epsilon'' \times 10^4$								
0.1 c/s	2.755	119	2.837	64	2.888	89	2.955	162	2.992	89
.2	2.750	135	2.835	67	2.884	82	2.947	169	2.988	100
.5	2.741	160	2.831	75	2.879	75	2.937	170	2.983	118
1	2.734	188	2.828	85	2.876	71	2.930	166	2.977	132
2	2.725	219	2.824	98	2.872	68	2.922	159	2.971	145
5	2.712	268	2.818	124	2.867	65	2.913	148	2.961	163
10	2.700	317	2.811	149	2.864	68	2.907	142	2.953	174
20	2.686	375	2.804	183	2.861	73	2.900	136	2.945	179
50	2.662	452	2.793	248	2.856	89	2.892	127	2.935	181
100	2.640	513	2.782	306	2.853	116	2.887	123	2.928	176
200	2.615	573	2.770	383	2.848	138	2.880	121	2.919	170
500	2.577	628	2.742	518	2.839	200	2.875	127	2.909	162
1 kc/s	2.548	647	2.715	628	2.831	266	2.869	136	2.902	158
2	2.514	632	2.689	731	2.820	359	2.864	158	2.895	161
5	2.478	575	2.642	857	2.795	539	2.856	211	2.886	171
10	2.453	505	2.597	880	2.764	695	2.847	283	2.880	191
20	2.433	429	2.556	860	2.729	878	2.837	396	2.873	234
50	2.408	351	2.500	764	2.670	1018	2.810	634	2.859	347
100	2.394	301	2.465	577	2.618	1086	2.778	850	2.848	496
200	2.383	260	2.442	587	2.564	1076	2.728	1070	2.829	715
310	2.375	235	2.426	540	2.538	1040	2.693	1175	2.811	880
1 Mc/s	2.362	184	2.390	423	2.466	811	2.601	1207	2.727	1222
3.2	2.351	152	2.365	336	2.412	609	2.515	1050	2.620	1282
10	2.338	125	2.343	270	2.374	465	2.448	840	2.523	1178
292	2.316	80					2.352	386		

smooth lines drawn through the points on such figures, the smoothed data presented in tables 2 to 5⁵ were obtained. The smoothed data are presented rather than the actual data in order to eliminate occasional points which are obviously excessively in error, as well as minimize the random effects of experimental error which arise from the limitations of the accuracy of the measuring apparatus. The experimental accuracy is discussed in detail in the appendix and is indicated in the legends of tables 2 through 6.

All the experimental loss index data have been corrected by subtracting out the loss component due to d-c resistance when this component exceeds 10^{-4} . The d-c resistance was determined by observing the current in the specimen after applying a d-c voltage.

⁵ In addition to the data reported in tables 2 and 3, measurements were made on specimen 0.80 at 90, 112, 136, and 160 °C and on specimen 0.44 at 105, 110, and 116 °C. The above measurements extended from 0.1 to 200 c/s. These points were used to determine activation energies and are not given in the tables.

The d-c resistance (R_{dc}) was computed from readings obtained after the observable time effects had vanished. In some cases this involved times of about 10^3 sec. The loss component due to the d-c resistance was computed from the equation

$$\epsilon''_{dc} = (\omega C_v R_{dc})^{-1} \tag{6}$$

where ω is 2π times f , the frequency. The low-frequency loss data are affected most by this component. Even so, at 0.1 c/s, ϵ''_{dc} was less than 10^{-4} for all specimens when the temperature was less than 100 °C. The loss data for specimen 0.44 required correction at 100 and 118 °C. Even at 118 °C, this correction was not required above 2 c/s, so that it scarcely altered the shape of the loss peak observed. Specimens 0.80 and 0.73 required correction only at temperatures at or above 175 °C. The loss data of the liquid specimen (200 to 250 °C), given in table 6,

TABLE 4. Smoothed dielectric data for specimen 0.12

The accuracies in ϵ' and ϵ'' are about 1% and 3% respectively

Temperature Frequency	-36.5 °C		-24.3 °C		-3.1 °C		22.7 °C		39.3 °C		47.8 °C		60.6 °C	
	ϵ'	ϵ''	ϵ'	ϵ''	ϵ'	ϵ''	ϵ'	ϵ''	ϵ'	ϵ''	ϵ'	ϵ''	ϵ'	ϵ''
0.02 c/s	2.462	249×10 ⁻⁴	2.514	234×10 ⁻⁴	2.612	199×10 ⁻⁴	2.750	127×10 ⁻⁴	2.840	97×10 ⁻⁴	2.886	100×10 ⁻⁴	2.982	195×10 ⁻⁴
.1	2.436	286	2.488	280	2.592	248	2.739	156	2.830	114	2.877	101	2.968	159
.2	2.423	299	2.476	301	2.582	273	2.732	177	2.825	128	2.873	107	2.965	150
.5	2.405	316	2.458	336	2.565	318	2.722	212	2.818	148	2.867	121	2.959	146
1.0	2.391	320	2.442	355	2.550	352	2.712	251	2.812	180	2.861	143	2.954	150
2	2.378	310	2.427	362	2.535	385	2.701	293	2.803	215	2.855	167	2.949	157
5	2.361	294	2.406	370	2.511	430	2.684	353	2.791	265	2.845	211	2.941	171
10	2.349	278	2.390	368	2.492	462	2.667	415	2.779	321	2.837	252	2.933	197
20	2.336	253	2.374	348	2.470	480	2.648	476	2.765	387	2.826	308	2.925	224
50	2.322	220	2.355	320	2.441	491	2.621	560	2.743	484	2.808	399	2.913	283
100	2.313	196	2.342	290	2.419	488	2.595	622	2.721	582	2.791	497	2.900	345
200	2.306	169	2.331	255	2.398	465	2.566	667	2.694	674	2.768	595	2.885	422
500	2.298	134	2.317	213	2.371	413	2.524	702	2.651	784	2.731	754		
1 kc/s	2.292	117	2.309	181	2.354	373	2.492	699	2.614	862	2.696	880		
2	2.287	100	2.302	154	2.339	325	2.461	666	2.574	902	2.654	978		
5	2.282	84	2.294	126	2.323	261	2.423	598	2.518	899	2.593	1058		
10	2.278	72	2.289	107	2.313	220	2.398	526	2.478	860	2.545	1062		
20	2.275	64	2.285	92	2.305	184	2.377	452	2.441	782	2.499	1010		
50	2.272	54	2.280	76	2.296	144	2.355	362	2.400	646	2.443	874		
100	2.270	50	2.277	68	2.290	130	2.342	310	2.374	562	2.407	767		
200	2.269	46	2.275	62	2.286	115	2.330	260	2.354	448	2.378	659		

TABLE 5.—Smoothed dielectric data for specimen 0.73

$\delta\epsilon'$ and $\delta\epsilon''$ are the possible error in the values of ϵ' and ϵ'' reported below. When $f < 100$ kc/s then $\delta\epsilon' = 0.4\%$ and $\delta\epsilon'' = 1.4\%$ and when $f > 100$ kc/s then $\delta\epsilon' = 1.5\%$ and $\delta\epsilon'' = 6.5\%$

Temperature Frequency	-36.2 °C		23 °C		50.6 °C		75 °C		92.7 °C	
	ϵ'	$\epsilon'' \times 10^4$								
0.1 c/s	2.594	241	2.752	60	2.788	24	2.823	84	2.856	103
.2	2.584	278	2.749	68	2.787	25	2.819	76	2.851	100
.5	2.566	325	2.743	84	2.786	26	2.815	67	2.846	95
1.0	2.551	359	2.740	102	2.785	29	2.812	61	2.841	92
2	2.534	380	2.735	121	2.784	36	2.809	55	2.837	88
5	2.509	384	2.728	154	2.782	48	2.806	51	2.833	84
10	2.491	369	2.721	191	2.780	60	2.804	50	2.828	80
20	2.473	345	2.713	231	2.778	77	2.802	50	2.826	77
50	2.453	297	2.698	300	2.773	113	2.800	54	2.821	72
100	2.440	257	2.684	366	2.767	152	2.798	63	2.818	71
200	2.430	220	2.667	430	2.760	202	2.796	77	2.815	71
500	2.418	178	2.637	505	2.747	290	2.792	106	2.811	76
1 kc/s	2.410	154	2.613	544	2.734	382	2.787	144	2.806	88
2	2.404	137	2.586	562	2.715	488	2.782	205	2.803	105
5	2.397	121	2.550	521	2.681	607	2.769	324	2.798	149
10	2.392	111	2.524	468	2.649	667	2.754	448	2.792	227
20	2.387	103	2.506	414	2.616	680	2.730	597	2.781	337
50	2.381	95	2.484	341	2.573	630	2.686	727	2.758	530
100	2.376	90	2.468	298	2.544	560	2.649	776	2.729	674
200	2.371	87	2.454	270	2.523	495	2.611	775	2.693	801
320	2.367	85	2.446	254	2.508	458	2.588	745	2.665	864
1 Mc/s	2.360	80	2.426	224	2.477	382	2.545	640	2.598	855
3.2	2.352	76	2.410	202	2.452	315	2.508	532	2.550	727
10	2.344	74	2.395	187	2.432	270	2.479	445	2.512	633
45			2.379	169						
100			2.371	160						

Temperature Frequency	108.4 °C		123.9 °C		148.9 °C		174.5 °C	
	ϵ'	$\epsilon'' \times 10^4$						
0.1 c/s	2.891	123	2.936	122	2.996	34	2.971	14
.2	2.885	121	2.930	126	2.992	42	2.970	12
.5	2.878	118	2.923	134	2.989	54	2.970	11
1.0	2.873	116	2.917	137	2.986	65	2.969	11
2	2.868	113	2.912	140	2.983	77	2.968	11
5	2.862	108	2.904	141	2.980	95	2.968	12
10	2.857	106	2.898	142	2.975	113	2.967	15
20	2.852	103	2.893	140	2.969	130	2.967	19
50	2.847	99	2.885	136	2.961	154	2.966	25
100	2.842	97	2.878	133	2.953	169	2.965	35
200	2.839	95	2.873	127	2.944	181	2.964	47
500	2.834	92	2.867	120	2.932	190	2.962	70
1 kc/s	2.830	91	2.862	116	2.923	190	2.958	94
2	2.826	97	2.856	114	2.915	186	2.953	125
5	2.821	120	2.849	121	2.905	178	2.942	170
10	2.817	154	2.844	132	2.897	175	2.933	198
20	2.811	209	2.839	152	2.888	175	2.924	211
50	2.799	340	2.831	223	2.879	188	2.909	221
100	2.784	490	2.825	319	2.872	227	2.901	228
200	2.761	686	2.809	469	2.865	295	2.894	267
320	2.741	802	2.795	608	2.857	380	2.888	311
1 Mc/s	2.675	945	2.744	930	2.831	600	2.871	493
3.2	2.603	910	2.676	1012	2.775	1000	2.832	847
10	2.545	825	2.600	965	2.702	1205	2.757	1180

TABLE 6. Dielectric data for specimen 0.0^a

Time sequence	1			2			3			4		
Temperature	243.1 °C			219.5 °C ^b			244.2 °C			197.6 °C		
Frequency	ϵ'	$\epsilon'' \times 10^4$	$\epsilon''_{dc} \times 10^4$	ϵ'	$\epsilon'' \times 10^4$	$\epsilon''_{dc} \times 10^4$	ϵ'	$\epsilon'' \times 10^4$	$\epsilon''_{dc} \times 10^4$	ϵ'	$\epsilon'' \times 10^4$	$\epsilon''_{dc} \times 10^4$
20 c/s	2.514	120	263	2.574	55	128						
50				2.574	23	51						
100	2.514	22	53	2.574	11	26	2.568	36	91	2.633	3	12
200	2.513	11	26	2.574	6	13						
1 kc/s										2.633	2	1
10										2.633	6	
160										2.632	16	

^a The accuracies of ϵ' and ϵ'' are about 0.5% and $\pm(1.5\% + 1 \times 10^{-4})$ respectively. Values of ϵ'' given above were obtained by subtracting the indicated contribution of the d-c conduction (ϵ''_{dc}) from the measured value of the loss index.

^b These specimens were in the supercooled liquid state.

required considerable correction, and the magnitude of the d-c component subtracted is included in table 6.

3.1. Data for Specimen 0.80. Nomenclature Used to Denote Loss Processes

Figures 2 and 3 show the frequency dependence of ϵ'' and ϵ' , respectively, at the indicated temperatures for specimen 0.80. These plots illustrate the behavior with temperature of the most prominent loss process in the polymer.

The loss process leading to the loss maximum evident in figure 2 will be called the "low-temperature" process, since on a plot of the loss index as a function of the temperature, T , at a constant low frequency, this effect occurs at temperatures lower than the other processes observed. Figure 4, in which ϵ'' at 1 c/s is plotted against T for the $\chi=0.80$ specimen, illustrates the scheme employed to name the loss processes observed in this polymer.

Considerable care will be taken in the paper to correlate and identify the loss peaks on the ϵ'' versus T plots, with the corresponding maximums (or other effects) in the appropriate ϵ'' versus $\log f$ plots. If a loss peak appears on an ϵ'' versus T plot, the underlying mechanism causing the peak will usually lead to a maximum or other discernible effect in an ϵ'' versus $\log f$ plot in the appropriate temperature and frequency range. In general, an analysis based on a study of both types of plot is more powerful than with just one or the other. It is emphasized that the nomenclature used to denote a process under discussion is based on the ϵ'' versus T plot (see fig. 4), irrespective of whether the process is manifested on an ϵ'' versus T plot or an ϵ'' versus $\log f$ plot.

Two other relaxation processes were observed in specimen 0.80. The first of these, on an ϵ'' versus

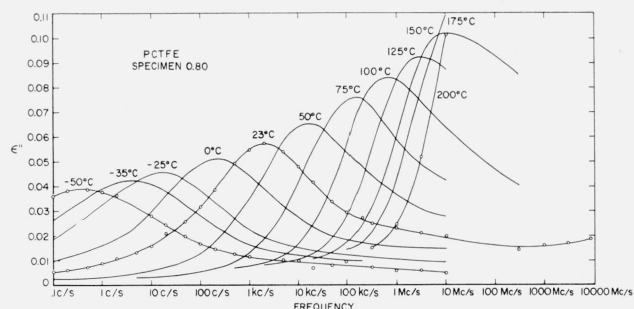


FIGURE 2. Frequency dependence of the principal loss index peak in specimen 0.80 as a function of temperature.

This peak corresponds to the low temperature peak on an ϵ'' versus temperature plot (see fig. 4).

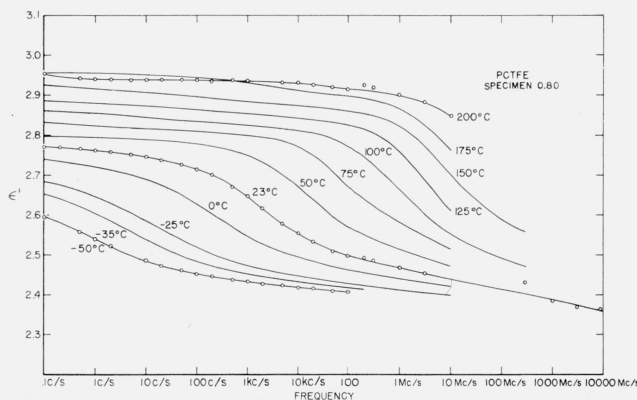


FIGURE 3. Dielectric constant versus frequency for specimen 0.80 as a function of temperature.

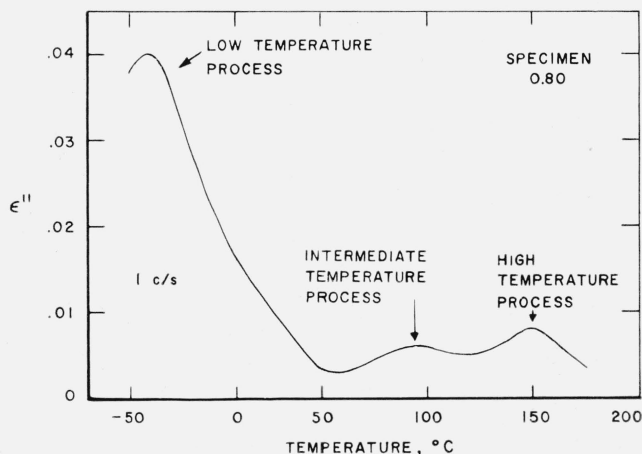


FIGURE 4. ϵ'' versus temperature at 1 c/s for specimen 0.80.

This illustrates the nomenclature scheme used to denote the loss processes.

$\log f$ plot (fig. 5), is most apparent in the temperature region between 75 and 125 °C at frequencies between 0.1 c/s and 10 kc/s. It is evident in figure 5 that a small loss maximum, partly obscured by other mechanisms, shifts from low frequencies on through the 10 c/s region to higher frequencies as the temperature is raised from 75 to 125 °C. This mechanism is the same as the one which leads to the clear-cut intermediate-temperature process peak when ϵ'' at a fixed (low) frequency is plotted as a function of temperature (fig. 4). Hence, this mechanism is denoted as the "intermediate-temperature" process.

The third relaxation process observed in the $\chi=0.80$ specimen shows up quite clearly on both an ϵ'' versus $\log f$ plot and an ϵ'' versus T plot. The loss peak in the ϵ'' versus $\log f$ plot shown in figure 6 is easily seen at 150 and 175 °C, but at

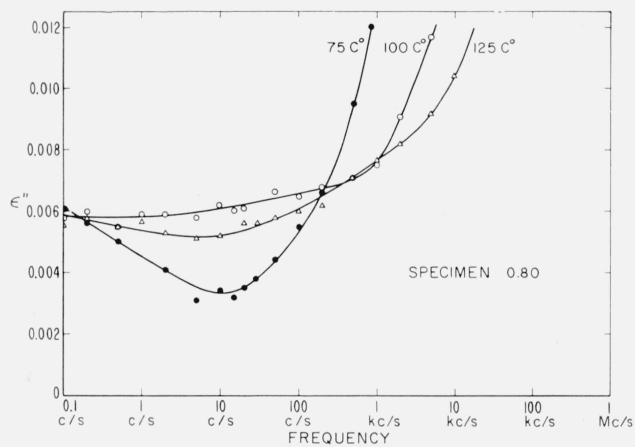


FIGURE 5. Loss index versus frequency showing evidence for the intermediate-temperature loss process in specimen 0.80.

Near 10 c/s, the loss is higher at 100 °C than at either 75 °C or 125 °C. This indicates that a small loss process traversed this region as the temperature increased. The loss mechanism causing this effect is the same as that which causes the intermediate temperature loss peak in figure 4.

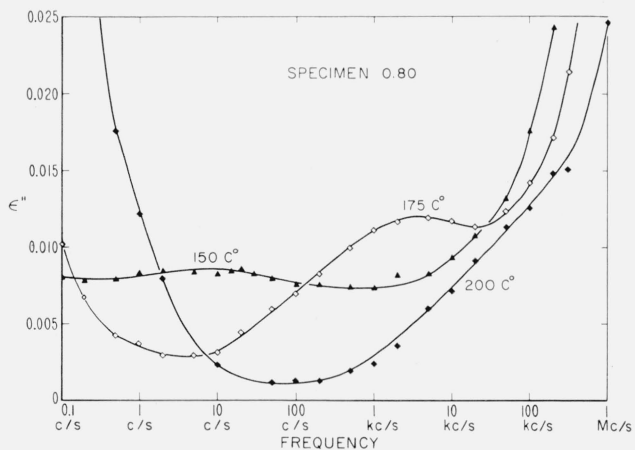


FIGURE 6. ϵ'' versus frequency at various temperatures showing the high-temperature loss process in specimen 0.80.

The loss process giving the maximum is the same as that which causes the high-temperature peak in figure 4.

The degree of crystallinity of specimen 0.80 changes at temperatures above 140 °C (see fig. 1). At 150 °C, 175 °C, and 200 °C the value of χ is 0.79, 0.75, and 0.65 respectively.

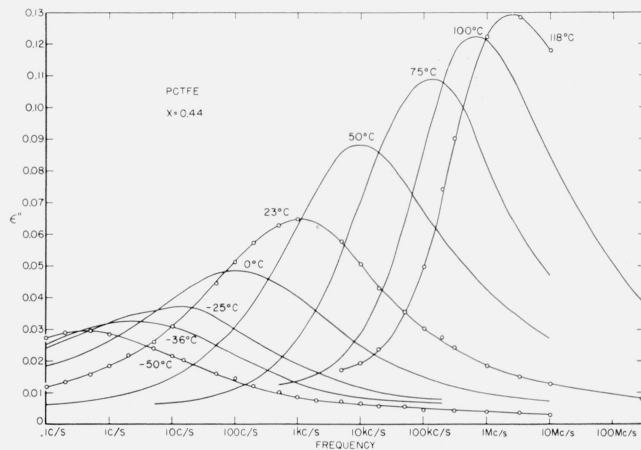


FIGURE 7. ϵ'' versus frequency at various temperatures for specimen 0.44.

This large loss peak is due to the low-temperature mechanism.

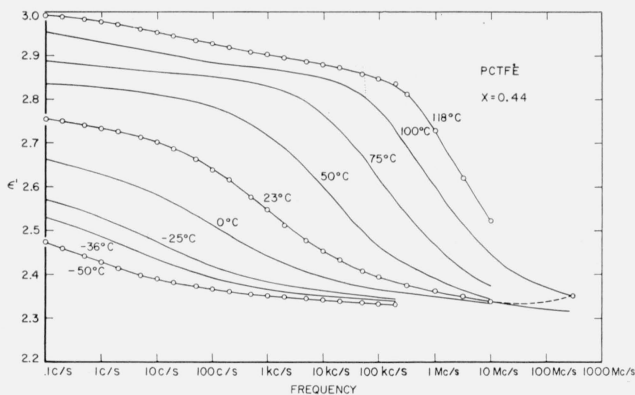


FIGURE 8. Dielectric constant versus frequency for specimen 0.44.

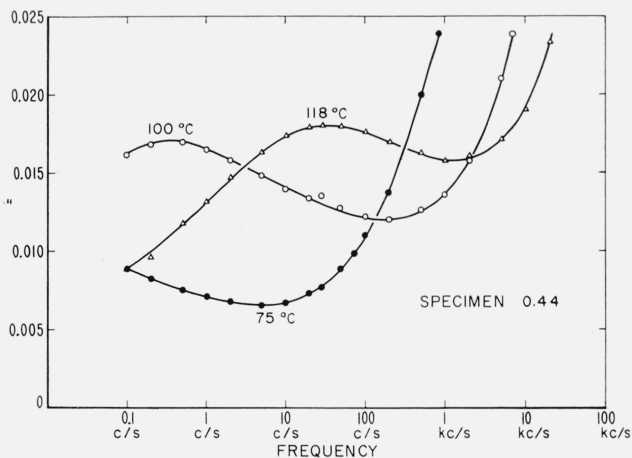


FIGURE 9. Frequency dependence of the loss index of specimen 0.44 at high temperatures and low frequencies.

The loss peak is mostly due to the intermediate-temperature mechanism, but contains some contribution from the high-temperature mechanism (cf. fig. 4).

200 °C it is obscured by the loss peak associated with the low- and intermediate-temperature processes. The mechanism leading to this loss peak is the same as that producing the high-temperature peak in the ϵ'' versus T plot (fig. 4). For convenience, this process, whether manifested in an ϵ'' versus T plot or an ϵ'' versus $\log f$ plot, is called the "high-temperature" mechanism.

3.2. Data for Specimen 0.44

The data for specimen 0.44 are presented in figures 7 and 8 where ϵ'' and ϵ' respectively are plotted as functions of $\log f$ at the indicated temperatures. From figure 7 it is apparent that the low-temperature relaxation process is active in this specimen.

Figure 9 shows the frequency dependence of the loss index in the high-temperature, low-frequency region. The loss index peak observed here is higher in magnitude than either the high-temperature process or the intermediate-temperature process evidenced in specimen 0.80. As will be discussed later, this loss peak is mostly due to an intermediate-

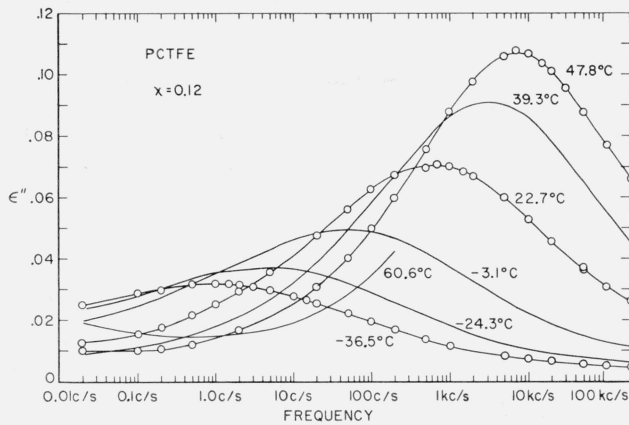


FIGURE 10. The frequency dependence of the loss index for specimen 0.12 (thin film).

These loss peaks are a result of the low-temperature process.

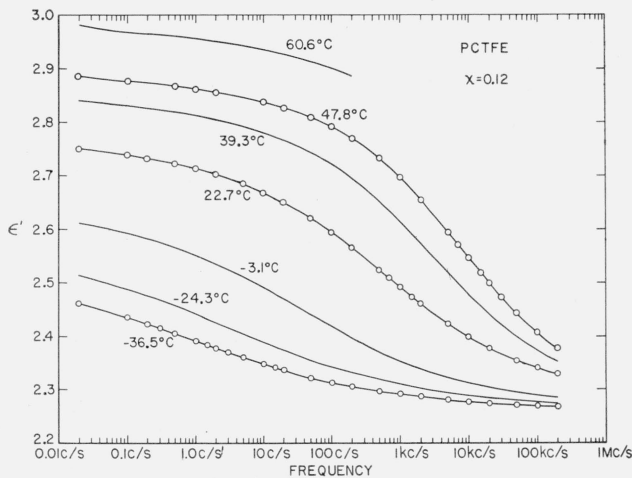


FIGURE 11. Frequency dependence of the dielectric constant of specimen 0.12.

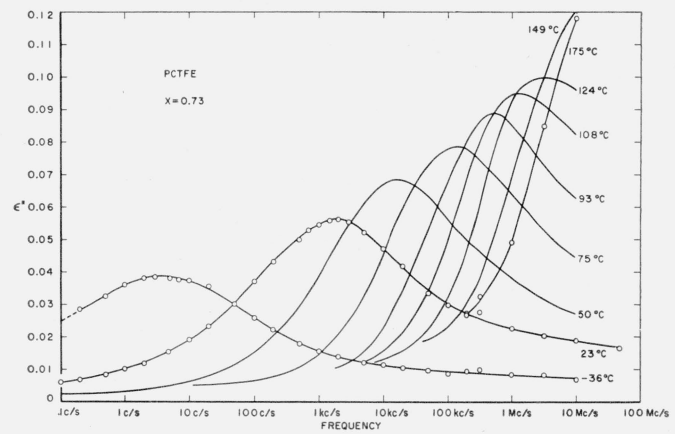


FIGURE 12. ϵ'' versus frequency at various temperatures for specimen 0.73.

The loss peaks are due to the low temperature mechanism.

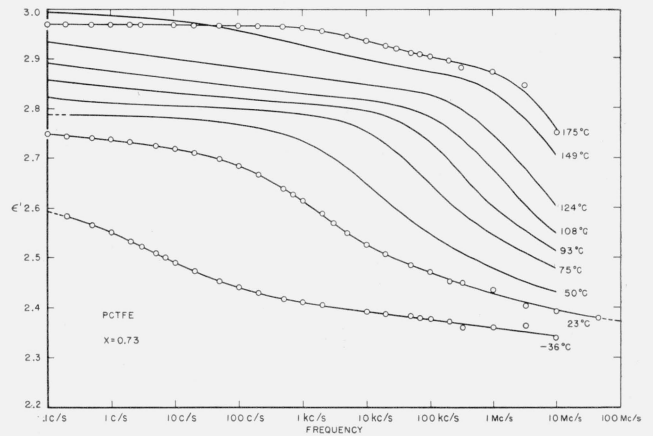


FIGURE 13. The dielectric constant versus the frequency for specimen 0.73.

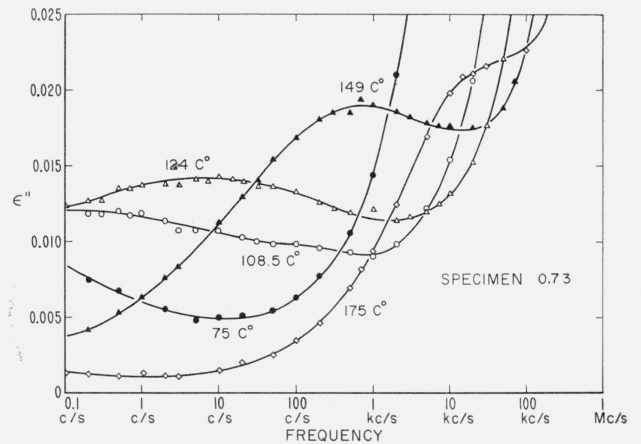


FIGURE 14. The frequency dependence of ϵ'' for specimen 0.73 at high temperatures and low frequencies.

The loss peaks are due to mixed intermediate and high temperature contributions (cf. fig. 4).

temperature mechanism of the type that appeared in the 0.80 specimen, but it evidently contains a contribution from the high-temperature loss mechanism. The peak in the ϵ'' versus $\log f$ plot that appears explicitly in figure 9 for $\chi=0.44$ is clearly substantially larger than that which exists (but which does not appear explicitly as a loss maximum in an ϵ'' versus $\log f$ plot) in the $\chi=0.80$ specimen (fig. 5).

3.3. Data for Specimen 0.12

Since this specimen was a thin film, special comments on the measurements are necessary. These are given in appendix 5.3. Broadly speaking, the error in the measurement of ϵ' and ϵ'' for the thin film is about ± 1 percent and ± 2 percent respectively. The measurements on the thicker disk-shaped specimens are substantially more precise (see appendix, and footnotes in tables 2, 3, and 5).

Figures 10 and 11 show ϵ'' and ϵ' versus frequency for specimen 0.12. On an ϵ'' versus T plot, to be discussed later, the data on 0.12 exhibits the low-temperature process.

3.4. Data for Specimen 0.73

Figures 12 and 13 present ϵ'' and ϵ' versus frequency at the indicated temperatures for specimen 0.73. The loss peak in figure 12 is associated with the low-temperature peak on an ϵ'' versus T plot, and is rather similar in character to that evident in specimens 0.44 and 0.80.

The loss index of specimen 0.73 as a function of frequency for various temperatures between 75 and 175 °C is presented in detail in figure 14. Later, it will be shown by the use of an ϵ'' versus T plot at 1 c/s that this loss maximum results from "mixed" contributions from both the intermediate- and high-temperature mechanisms.

It is appropriate at this time to recall that specimen 0.73 was prepared by annealing a previously quenched bulk specimen at 190 °C until a high degree of crystallinity was achieved ("quench-anneal" technique). This was done in order to compare the dielectric properties of specimens with nearly the same high degree of crystallinity, but with crystals nucleated and grown under different conditions. The most striking difference between the dielectric properties of specimens 0.73 and 0.80 occurs in the high-temperature, low-frequency region. Comparison of figures 6 and 14, particularly the data obtained near 175 °C, demonstrates this difference most effectively. Figure 6 shows a loss peak maximum for specimen 0.80 ($\chi=0.75$ /at 175 °C as noted in fig. 1) at 175 °C near 1.5 kc/s, while figure 14 shows a loss peak maximum for specimen 0.73 at 175 °C near 15 kc/s. The one-decade shift in the frequency location of this loss peak in the two specimens indicates that even though two specimens may have the same degree of crystallinity, their dielectric properties need not be identical. The cause of this effect will be discussed in section 4.1c.

3.5. Empirical Method of Estimating χ From the Dielectric Data

In order to correlate and compare the dielectric data of PCTFE presented here with results obtained previously by others, it is necessary to know approximately the degree of crystallinity of the specimens that they used. In many cases, the density of the specimen was not reported in the literature, so that this means of estimating the degree of crystallinity cannot be employed. However, at least a rough value of the degree of crystallinity can be obtained from the dielectric data itself.

To facilitate this determination, a convenient although crude crystallinity "scale" was obtained from our dielectric data on specimens of known χ . Comparison of our room-temperature data for specimens of various degrees of crystallinity showed that in the most commonly employed frequency region (about 50 c/s to 100 kc/s), the loss index at about 100 c/s exhibited the greatest dependence upon χ . The dependence of the 100 c/s values of ϵ'' and $\tan \delta$ upon the degree of crystallinity is presented in figure 15. The degree of crystallinity of specimens employed in other dielectric investigations of PCTFE was estimated from the curves of figure 15. The results are given in table 7. In most cases, the

TABLE 7. Estimated degree of crystallinity of PCTFE specimens used in other dielectric studies^a

Author	Specimen description	χ dielectric method	χ density method
Reynolds and coworkers [1]	"Kel-F" polymer.....	0.47	-----
Hartshorn and coworkers [2]	(1) cooled slowly from 250 °C.....	.60	-----
	(2) quenched from 210 °C.....	.54	-----
	(3) quenched from 250 °C.....	.40	-----
Mikhailov and Sazhin [3] ^b	(1) cooled slowly.....	0.65	-----
	(2) abruptly cooled.....	(~0.2)	-----
Nakajima and Saito [6]...	(1) cooled slowly from melt.....	.52	0.48
	(2) quenched to room temperature.....	.47	.46
	(3) quenched to -30 °C.....	(~0.3)	.43

^a Except where noted, the values of χ (dielectric method) were estimated from the dielectric loss data using the crystallinity "scale" given in figure 15. The χ (density method) values were calculated from the densities (when given), using the crystallinity scale of reference [4].

^b χ estimated from 23 °C $\tan \delta$ data at 50 c/s.

values of χ obtained by the dielectric method are compatible with the indicated thermal history of the specimen. However, the values of χ obtained for the "abruptly cooled" specimen of Mikhailov and Sazhin, and for the "quenched to -30 °C" specimen of Nakajima and Saito, appear to be lower than one would expect from the indicated thermal treatment *assuming* that bulk specimens were employed. (Nakajima and Saito used specimens 2 mm thick.)

Even with the most stringent quenching techniques we have been unable to attain such low values of χ except with thinner specimens. While the results in table 7 for the dielectric method doubtless give a rough picture of the range of χ used by other

investigators, it is clear that χ determinations based on ϵ'' or $\tan \delta$ measurements on PCTFE must not be regarded as being a substitute for the more accurate density method.

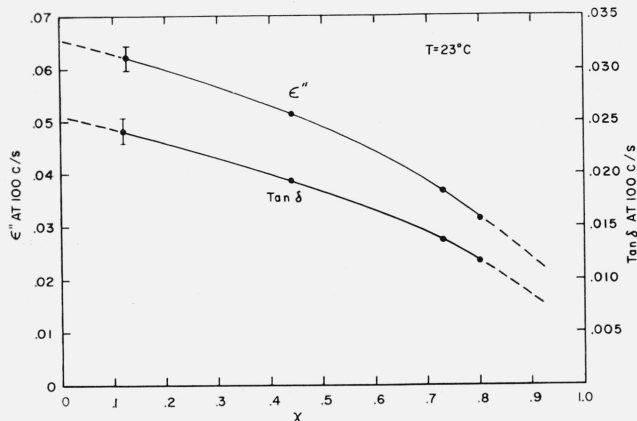


FIGURE 15. The 100 c/s values of the loss index and $\tan \delta$ at room temperature as a function of the degree of crystallinity.

These data are intended to provide an approximate crystallinity scale for dielectric specimens where the specific volume has not been reported.

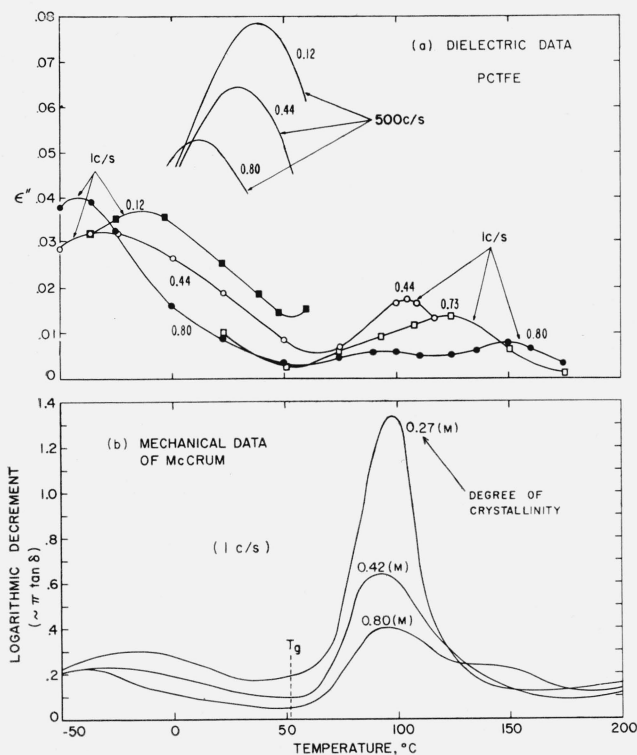


FIGURE 16. Direct comparison between dielectric and mechanical loss data.

a. The temperature dependence of the loss index at 1 c/s and 500 c/s for specimens of various crystallinities. b. The temperature dependence of the mechanical loss at 1 c/s for specimens of various crystallinities. The data at 1 c/s provide a direct comparison of the dielectric and mechanical data. The 500 c/s dielectric data illustrate the shift of the maximums with increasing f .

4. Interpretation of Results

4.1. The Intermediate- and High-Temperature Relaxation Processes

The principal objective of this section is to identify the phases in which the intermediate- and high-temperature loss processes originate, and to consider the nature of the relaxation phenomena in these phases. It will be demonstrated in section 4.4 that none of the dielectric loss peaks discussed are a result of Maxwell-Wagner polarization.

a. The Intermediate-Temperature Process

In discussing the intermediate-temperature loss process, use will be made of the dynamic mechanical loss data on PCTFE of McCrum⁶ [8], who studied specimens of various degrees of crystallinity. Although others [9, 10, 11] have studied the dynamic mechanical properties of PCTFE, the data of McCrum are particularly valuable since he investigated specimens with a wide range of known crystallinities.

A useful type of plot in discussing the dielectric aspects of the intermediate-temperature loss process is shown in figure 16a, where ϵ'' is plotted as a function of temperature at 1 and 500 c/s for the various dielectric specimens. A graph of the mechanical loss data of McCrum, plotted as logarithmic decrement ($\approx \pi \tan \delta$) versus temperature, also at 1 c/s, for samples of various degrees of crystallinity is shown in figure 16b.⁷ The degree of crystallinity was calculated from specific volume data using eq (5).

Three mechanical loss peaks are evident in specimen 0.80(M) ($\chi=0.80$). The intermediate-temperature peak is in general most pronounced and occurs at virtually the same temperature (95 °C) in all three specimens. The intermediate peak observed dielectrically in specimen 0.80 at 1 c/s also occurs near 95 °C. This suggests that the same molecular relaxational mechanism underlies both the mechanical and the dielectric intermediate-temperature loss peak. Since the magnitude of the mechanical intermediate-temperature peak is increased by increasing the fraction of the amorphous phase present (see fig. 16b), it seems reasonable to identify this peak tentatively as a property of the normal amorphous (supercooled liquid) component of the semicrystalline polymer. Further evidence supporting this identification will be presented shortly.

The intermediate peak in the dielectric data evidently decreases in magnitude as the fraction of the amorphous component decreases. (Compare 0.80 and 0.44 curves in fig. 16a). This decrease of intensity can be clearly discerned despite the fact there is evidently some "mixing" of the main intermediate component and a weaker high-temperature process

⁶ The authors are deeply indebted to Dr. McCrum of the E. I. duPont de Nemours Company for making these data available to us prior to publication.

⁷ Dr. McCrum has measured the logarithmic decrement ($\pi \tan \delta$) and the torsion modulus G , at 1 c/s using the torsion pendulum method at temperatures between -180 and +210 °C. Since no further mechanical loss maximums were observed below -50 °C and our dielectric data does not extend below -50 °C, only the $\pi \tan \delta$ data above -50 °C are shown here.

component in specimen 0.44 which causes an upward shift of the characteristic temperature. (A detailed discussion of this shift is given in section 4.1c. The peak for 0.73, which was crystallized in a very different manner than 0.80, is so completely "mixed" and strongly shifted as to be of little value in the present comparison.) In any case, the relative intensities of the dielectric loss peaks at 1 c/s for 0.44 and 0.80 in the vicinity of 90 to 105 °C clearly suggest that the amorphous phase is the seat of the intermediate process.

It will now be demonstrated that the intermediate-temperature loss mechanism that appears at about 95 °C at 1 c/s in both the dielectric and mechanical data may reasonably be associated with the relaxational effects of the normal glass transition in the amorphous regions of the polymer at $T_g=52$ °C.

A typical property of the onset of the glass transformation in an entirely amorphous body is that the apparent heat of activation, ΔH^* , decreases rapidly as the temperature is increased above T_g . From the work of Williams, Landel, and Ferry (WLF) [12], this dependence of ΔH^* on temperature is given for many amorphous substances, including noncrystalline linear polymers, by the empirical expression

$$\Delta H^*(\text{cal/mole}) = \frac{4.12 \times 10^3 T^2}{(51.6 + T - T_g)^2} \quad (7)$$

where T_g is the glass transformation temperature as determined from the break in a specific volume versus temperature ($\bar{V}-T$) plot. Ferry [13] has indicated that the constants in this expression may vary somewhat from one case to another, but eq (7) is still to be regarded as a fair representation of the general situation. The expression is valid between T_g and $T_g + 100$ °K.

The apparent heat of activation was calculated from the data using the expression

$$\frac{-R \partial \ln f_m}{\partial (1/T)} = \Delta H^* \quad (8)$$

where R is the gas constant, T the absolute temperature, and f_m the frequency of the maximum in an ϵ'' versus $\log f$ plot. In some cases, eq (8) was used over restricted temperature ranges to obtain ΔH^* as a function of temperature.

Figure 17 shows a plot of $\log f_m$ versus $1/T$.

Specimen 0.80 was the only specimen for which the maximum of the intermediate-temperature peak on an ϵ'' versus $\log f$ plot was sufficiently resolvable. The $\chi=0.44$ specimen exhibits a peak mostly due to the intermediate process (figs. 9 and 16), but the shift of f_m with $1/T$ due to the intermediate component itself is not accessible.⁸

The apparent heats of activation associated with the intermediate-temperature process for the 0.80 specimen are given for two temperatures in table 8.

⁸ An attempt was made to observe the intermediate-temperature process in specimen 0.12. Upon warming the film above about 60 °C, however, further crystallization took place. A loss peak ($\epsilon''_{\text{max}}=0.0243$) was ultimately observed at 0.08 c/s at 92 °C. The degree of crystallinity of the specimen had by then increased to 0.34.

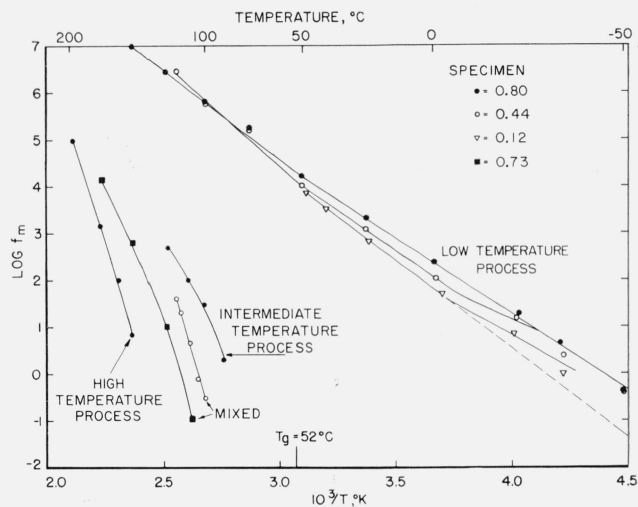


FIGURE 17. Frequency of the maximums of the loss peaks, f_m , versus the reciprocal of the absolute temperature.

The points were obtained from the ϵ'' versus $\log f$ plots.

TABLE 8. Apparent heats of activation for the various dielectric relaxation processes^a

Low-temperature process			
Specimen	χ	Temperature range	ΔH^* , kcal/mole
0.80	0.80	-50 to 50 °C	14.6±5%
.44	.44	0 to 50 °C	15.8±5%
.12	.12	0 to 50 °C	16.7±5%
Resolved intermediate-temperature process			
0.80	0.80	Near 90 °C	67±20%
.80	.80	Near 120 °C	34±20%
Mixed-intermediate and high-temperature process			
0.73	0.73	Near 115 °C	95±20%
.73	.73	Near 160 °C	49±20%
.44	.44	100 to 118 °C	80±20%
Resolved high-temperature process			
0.80	0.79	Near 150 °C	91±20%
.80	.68	Near 190 °C	70±20%

^a All heats of activation were calculated from data obtained from ϵ'' versus $\log f$ plots.

Despite the fairly large uncertainty, it is evident that ΔH^* decreases rapidly as the temperature is increased above T_g . (ΔH^* drops from 67 to 34).⁹

The temperature dependence of the apparent heat of activation for the intermediate-temperature process calculated using the dielectric data is in fairly good agreement with that calculated from the WLF expression, eq (7), with $T_g=52$ °C. This is illustrated in figure 18. The fact that some difference exists between the predicted and experimental values of ΔH^* in this case is not surprising, since

⁹ While the experimental points determining the $\log f_m$ vs. $1/T$ curve for the intermediate process of specimen 0.80 (fig. 17) may possibly be fitted by a straight line, the curved line shown in figure 17 provides a far better fit of all the points. Furthermore, a curved line is to be expected in this case on the basis of experimental work of others [14, 48].

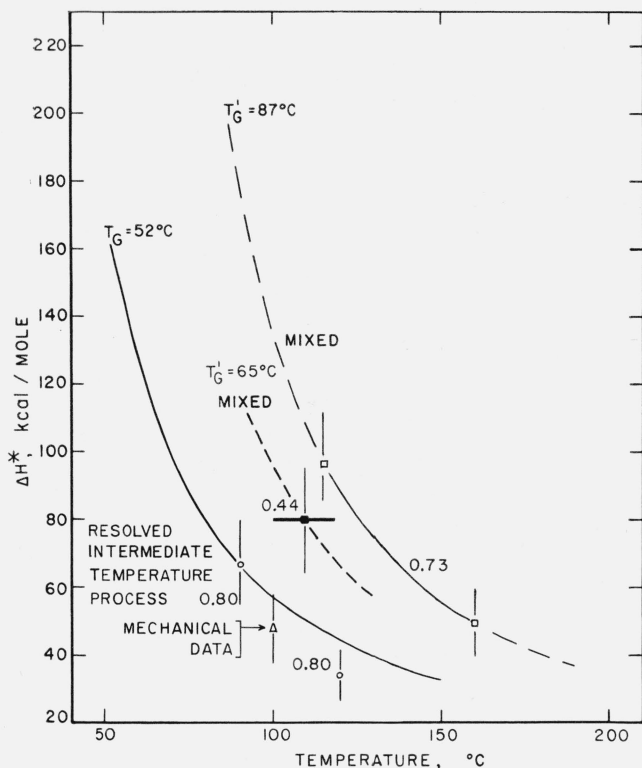


FIGURE 18. The apparent activation energy of the intermediate-temperature process and mixed intermediate- and high-temperature processes versus the temperature.

The curved lines were calculated from the WLF equation, using the indicated values for T_g or T_g' .

The points (except one) indicate the experimental dielectric data. The single mechanical point results from combining the 1 c/s data of McCrum [8] with the 3.3 c/s data of Schmieder and Wolf [9].

the accuracy with which ΔH^* is experimentally determined is rather low, and since the constants in eq (7) are not strictly universal.

Also shown in figure 18 is a single point calculated from the difference in location of the 1 c/s mechanical loss peak at 95 °C observed by McCrum, and the 3.3 c/s mechanical peak at 104 °C observed by Schmieder and Wolf [9]. Although this point was calculated from two different sets of data, and from a temperature rather than a frequency plot, it is consistent with the points obtained from the dielectric data for the intermediate-temperature process and falls fairly close to the curve calculated from eq (7).

The fact that the WLF expression is obeyed even approximately (with $T_g = 52$ °C from $\bar{V}-T$ data) for the resolved intermediate process indicates that this process is a relaxation effect that is premonitory to the glass transition that occurs at 52 °C.

Another indication that the intermediate process is associated with the glass transition is provided by the large change of modulus in the mechanical data in the general vicinity of the intermediate peak, especially in the less crystalline specimens. Strictly amorphous polymers show a similar large change of modulus.

When considered together, the facts outlined above lead to the definite conclusion that the intermediate-temperature process is indeed a bulk property of the amorphous (supercooled liquid) component of the polymer, and further, that this process is due to relaxation effects connected with the onset of the normal glass transition in these amorphous regions. The molecular phenomena leading to the intermediate-temperature process doubtless involve complex motions of a large number of polymer chain segments in the amorphous phase.

Saito and Nakajima [14] have experimentally demonstrated in the amorphous polymers they studied that the frequency of the loss index maximum for the relaxation peak associated with the glass transition lies between 10^{-2} and 10^{-3} c/s, when the temperature of the specimen is at the value of T_g determined from the break in the $\bar{V}-T$ plot. Using a linear extrapolation of the $\log f_m$ versus $1/T$ data for the intermediate-temperature peak in specimen 0.80, one obtains $T = 57$ °C when $f = 10^{-2}$ c/s and $T = 47$ °C when $f = 10^{-3}$ c/s. The value of T_g (52 °C) does indeed lie between these temperatures. There are, however, several difficulties with this simple extrapolation in the case of PCTFE. The $\log f_m$ versus $1/T$ line is actually curved, and both of the above estimates of T are low in comparison with what is estimated using curvature (see below). The extrapolation is in any case rather long. Using an extrapolation with our best estimate of the curvature, it is estimated that $T = 77 \pm 10$ °C for 10^{-2} c/s and $T = 72 \pm 10$ °C for 10^{-3} c/s, both values being higher than the value $T_g = 52$ °C obtained from $\bar{V}-T$ data. While the above may be regarded as providing general though not conclusive support for our previous conclusion that the intermediate-temperature process is connected with the glass transition in the amorphous component, it is apparent that extrapolation to frequencies well below 10^{-3} c/s would be required to give a T value that corresponded to T_g from the $\bar{V}-T$ data in the case of this semicrystalline polymer.

One possible explanation of the different f values (on a $\log f_m$ versus $1/T$ plot) that correspond to T_g , as measured by the $\bar{V}-T$ method, in purely amorphous polymers ($f = 10^{-2}$ to 10^{-3} c/s) on the one hand, and the amorphous component of semicrystalline polymers ($f \ll 10^{-3}$ c/s) on the other, is that the T_g value from the $\bar{V}-T$ data in an entirely amorphous polymer is considerably more time-dependent than it is in a semicrystalline polymer.

Saito and Nakajima have shown that T_g from $\bar{V}-T$ data depends on the rate of measurement in purely amorphous polymers, being higher the more rapid the measurement [14]. Interestingly, the same authors have shown that T_g for a semicrystalline polymer, as measured by the $\bar{V}-T$ method, is much less sensitive to the time scale of the measurement. (This accords with our experience on $\bar{V}-T$ measurements of T_g with PCTFE). The implication is that the T_g value measured for a semicrystalline polymer by the $\bar{V}-T$ method is lower and nearer the intrinsic (quite possibly time-independent) value than that of a corresponding purely amorphous polymer. One possible explanation of this is that it is a result of a size effect, the amorphous regions in semicrystalline polymers being quite small. In any event, it would appear that in semicrystalline systems, f values that are substantially less than 10^{-3} c/s may be more appropriate in estimating values of T for comparison with T_g values from $\bar{V}-T$ data.

b. The High-Temperature Process

When clearly resolved on an ϵ'' versus T (dielectric) plot or a $\pi \tan \delta$ versus T (mechanical) plot, the high-temperature process peak appears at about 150 °C at 1 c/s (fig. 16). Notice that the resolved high-temperature peak appears only in the $\chi = 0.80$ specimens in both the dielectric and mechanical cases;

there is no indication of a resolved peak in specimen 0.73 (dielectric), which has practically the same degree of crystallinity at the temperature under consideration. Dielectric specimen 0.73 merely exhibits a single "mixed" high and intermediate peak. Further, no resolved high-temperature peak appears in mechanical specimens 0.27(M) or 0.42(M). This implies that the appearance of a resolvable high-temperature process not only involves the crystals in some way, but also depends on the manner in which the high crystallinity is achieved.

The crystallization in specimen 0.80 is of the typical lamellar spherulitic type. Large lamellar spherulites commonly appear in linear polymers crystallized from the melt under conditions of low to moderate supercooling such as was used in forming specimen 0.80 (section 2.2), and observations with a polarizing microscope fully confirm the existence of such objects in PCTFE specimens similar to 0.80 [15]. The milky-white appearance of specimen 0.80 is due to the scattering of light from these objects. Specimen 0.73, crystallized by the quench-anneal technique (sec. 2.2), is optically much clearer than 0.80, and contains no spherulites visible with a polarizing optical microscope. The same is true of specimen 0.44. The crystals (or spherulites) in 0.73 and 0.44 are evidently much smaller than in 0.80. In any case, it appears that the resolved high-temperature process evident in specimen 0.80 is closely associated with large and well-formed lamellar spherulites.

To an approximation sufficient for the present discussion, lamellar spherulites consist of stacks of chain-folded bladelike crystals (lamellae) that emanate from a central point (fig. 19). The long axes of the polymer molecules are essentially perpendicular to the two large flat faces of each blade, these faces containing the chain folds. In many cases, the lamellae are twisted as shown in figure 19. This twist leads to the beautiful bands that are seen in the optical extinction patterns of spherulites. The lamellae are commonly from 100 to 500Å thick (distance between plane of chain folds), this thickness being larger the higher the crystallization temperature. A general theory of the formation of chain-folded lamellar spherulites has been given by Hoffman and Lauritzen [16].

If the high-temperature process were a "glass transition" type of effect, a break in the $\bar{V}-T$ curve in the vicinity of about 120 °C would be expected. A careful examination of the $\bar{V}-T$ curve of specimen 0.80 reveals no obvious break above the one at $T_g=52$ °C, though lack of sensitivity might possibly be the cause of its apparent absence. Also, the WLF expression with an elevated glass transition temperature (~ 118 °C) is not necessary to explain the apparent temperature dependence of ΔH^* for the resolved high-temperature process (table 8); the assignment of the constant value $\Delta H^*=80$ kcal/mole provides an equally acceptable fit within the rather large experimental error. These observations, though not conclusive, are consistent with the proposal that the high-temperature process in PCTFE involves the crystal lamellae.

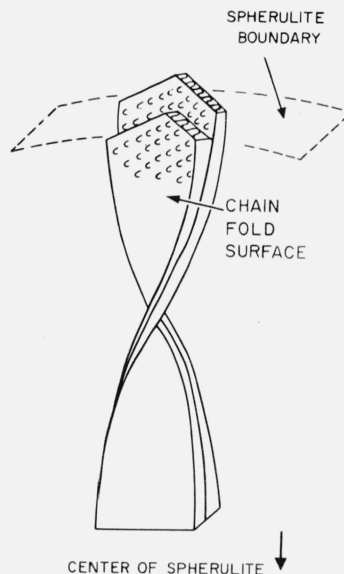


FIGURE 19. Chain-folded lamellar structure in spherulites (schematic).

There is some indication that the high-temperature process is not simply a property of the bulk crystalline phase.

If the high-temperature process were a bulk crystal property, it might be expected to appear in resolved form in specimen 0.73 with nearly the same intensity as it does in 0.80, whether or not the crystallization involved was of the well-formed lamellar spherulitic type. This is not the situation for the dielectric data. It may therefore be concluded that the high-temperature process is not a simple bulk property of the interior part of the crystals. This suggests that the high-temperature mechanism exhibited in resolved form by specimen 0.80 may involve the chain-folded surfaces of the lamellae. Crystal-size effects may be involved in shifting the high-temperature process to lower temperatures in 0.73, but this is not inconsistent with the general notion that lamellar surfaces or interlamellar surface interactions are involved. Also, the possibility exists that "abnormal" amorphous polymer contiguous to the crystal surfaces may be involved in the high-temperature process. This would place part of the cause of this process in the category of a lamellar-crystal-amorphous-phase interaction, but in a broad sense such an effect could still be regarded as a surface property.

In summary, the authors consider that a strong case exists for believing that the high-temperature process in its resolved form in PCTFE (specimen 0.80) is connected with the existence of well-formed lamellar chain-folded spherulitic structures. While it is not completely certain, some evidence suggests that the mechanism involves the surfaces of the lamellae.

Takayanagi has recently proposed that the high-temperature process, as observed in mechanical loss measurements in certain semicrystalline poly-

mers, is associated with chain-folded lamellar structures [17]. Resolved high- and intermediate-temperature peaks appear in the mechanical loss data of polyethylene and polyoxymethylene [18]. (These polymers also exhibit the low-temperature process).

A number of mechanisms can be proposed that might lead the crystals or their surfaces to exhibit dielectric and mechanical loss of the type observed in the high-temperature process. Broadly speaking, these mechanisms deal with motions of various types of surface (or other) defects in the lamellar crystals, motions of the chain folds, and interlamellar interactions, together with certain combinations of these concepts. However, the present experimental study does not point clearly to which if any of these ideas is correct, so no discussion of the various models is given.

c. Mixed Intermediate- and High-Temperature Processes

In figure 16a, it is seen that the dielectric loss peak that appears above 100 °C exhibits a large shift toward higher temperatures ($T \approx 105$ to $T \approx 125$ °C) as the degree of crystallinity increases from 0.44 to 0.73. Also, it is clear in the case of specimen 0.73 that only a single "mixed" peak appears, rather than two resolved peaks as in specimen 0.80. (Specimen 0.44 was not measured above 118 °C, but presumably has no resolved high-temperature process.) Recall again that specimens 0.44 and 0.73 do not contain large and well-formed spherulites, and that unlike 0.80, they were crystallized either during or subsequent to quenching.

The corresponding mechanical loss data for PCTFE plotted as $\pi \tan \delta$ versus T at 1 c/s do not exhibit such an obvious shift. Even when plotted as J'' (shear loss compliance) versus T , the loss peak shows no upward shift (within an error of about 5 °C) as χ is increased from 0.27 to 0.42. These specimens are similar to dielectric specimens 0.44 and 0.73 in being nonspherulitic,¹⁰ and in exhibiting only a single "mixed" loss peak. All were crystallized by the "quench crystallized" or the "quench→anneal" technique.

The above-mentioned upward shift of a single dielectric loss maximum with increasing χ in quenched or quench→annealed specimens might seemingly be interpreted as a large and genuine increase in the glass transition of the amorphous phase that is induced by the presence of crystals. One objective of this section is to indicate that the large upward shift in the dielectric case is *not* indicative of an equally large increase of T_g as measured from \bar{V} - T curves. A simple alternative explanation of the shift of the dielectric loss peak is proposed, and the negligible shift in the mechanical case discussed. Also, further cause will be given for the necessity of distinguishing between polymers crystallized from the melt, where well-formed lamellar spherulites appear, and by the quench or

quench→anneal technique, where in many cases obviously spherulitic crystallization does not arise. Brief mention is also made of crystallization in oriented systems.

The shift of the *apparent* glass transition, T_g' , for dielectric specimens 0.44 and 0.73 implied by the ϵ'' versus $\log f$ data may be estimated by applying the WLF expression for ΔH^* . T_g' is taken as that temperature which provides the best fit of the observed temperature dependence of ΔH^* with the WLF expression (fig. 18). The WLF expression was originally proposed for purely amorphous materials rather than semicrystalline ones, so this use of it here must be viewed with caution. Nevertheless, it will be recalled that it applies reasonably well to the resolved intermediate component of 0.80. If there is "mixing" of the amorphous (intermediate) process and a crystal (high-temperature) process in 0.44 and 0.73, then only an apparent (T_g') value of the glass transition may be expected.

Regarding the normal amorphous material with $T_g = 52$ °C as the reference point, T_g' for specimen 0.44 by the WLF method apparently shifts by 65 °C - 52 °C = 13 °C, and the shift exhibited by 0.73 is 87 °C - 52 °C = 35 °C.

An analysis using the $\log f_m$ versus $1/T$ plots also implies that the apparent value of the glass transition associated with the "mixed" peaks increases as the degree of crystallinity increases from 0.44 to 0.73. This is evident in figure 17, where it is seen that for any given f value, T is higher for $\chi = 0.73$ than it is for 0.44. However, as noted in section 4.1a, it is not easy to get a close estimate of the value of the apparent glass transition in these cases because of the curvature, and the uncertainty of the f value that should be used.

The concept that these large differences represent a real upward shift in the glass transition of the magnitude indicated is not substantiated by careful measurements of the glass transition temperature from changes of slope in the \bar{V} - T curves. With an error of less than 5 °C, specimens 0.44, 0.73, and 0.80 exhibit the same T_g value on \bar{V} - T curves.¹¹

It is therefore clear that the large upward shifts of the apparent glass transitions T_g' implied by the dielectric data are not to be regarded as real increases of the glass transition in the amorphous phase due to the presence of crystals. Recall also the fact that the mechanical data on specimens 0.27(M), 0.42(M), and 0.80(M) imply a small if not negligible increase of T_g with increasing χ . This is consonant with the \bar{V} - T measurements of T_g , which indicate a shift of between zero and about 5 °C for χ values between 0.44 and 0.80.

The disparity in the small if not negligible shift of T_g indicated by the mechanical and \bar{V} - T data on the one hand, and the large shift implied by the dielectric data on the other, can be explained at

¹⁰ The use of the term "nonspherulitic" here means that no *large* well-formed spherulites visible with a polarizing optical microscope appear in the specimens. It is not intended to imply that numerous extremely small lamellar spherulites, or small and somewhat disoriented lamellae, may not exist in the specimens.

¹¹ The somewhat compressed scale employed in the \bar{V} - T curves of figure 1 does not show the break near 52 °C to great advantage. A more detailed presentation of data on specimens similar to 0.44 and 0.80 is given in reference [4] and clearly reveals the glass transition effect. The \bar{V} - T data for specimen 0.73 has not been previously published.

least in part as follows. Comparing dielectric specimen 0.80 and mechanical specimen 0.80(M) in figure 16, it is seen that the high-temperature peak in the dielectric case is slightly more prominent than the intermediate peak, while in the mechanical case it has a considerably lower relative intensity. If in some type of specimen the high-temperature peak shifts downward a certain number of degrees and "mixes" with the intermediate peak to form a single broadened peak, one would expect the maximum in this resultant single peak to occur at higher temperatures in the dielectric than the mechanical case because of the aforementioned relative intensity difference. This explanation is consistent with the large upward temperature shift of the single maximum in the "mixed" dielectric cases $\chi=0.44 \rightarrow \chi=0.73$, and the corresponding much smaller shift in the mechanical case $\chi=0.27 \rightarrow \chi=0.42$ (see fig. 16). A careful examination of the dielectric and mechanical data for these specimens, as compared with the 0.80 specimens, definitely suggests a downward temperature shift has occurred in the high-temperature mechanism in the nonspherulitic specimens. This downward shift in the high-temperature process may tentatively be ascribed to a crystal-size effect, much smaller and disoriented lamellae appearing in specimens 0.27(M), 0.42(M), 0.44, and 0.73 than in the typically lamellar spherulitic specimens 0.80 and 0.80(M).

The general question of the possible cause of a true shift of T_g due to increasing crystallinity is a most interesting one. As noted above, the actual upward shift in T_g of PCTFE specimens 0.44 and 0.73 is certainly not over about 5 °C as measured from \bar{V} - T data. Similarly, the mechanical data for 0.27 (M) and 0.42(M) imply the shift in the loss peak is not any larger than this, and quite possibly less.

Two effects could account for a true increase of T_g in the amorphous phase: (1) It has been shown by Gee and coworkers [19] that stress elongation (*circa* 250%) in an amorphous polymer can increase T_g as measured by the \bar{V} - T method by 1 to 7 °C, depending on the polymer. This shows that molecular orientation of the liquid phase could increase T_g somewhat. (2) Typical bundlelike crystallization, where one polymer molecule participates in many crystallites, might possibly occur to some extent in quenched specimens. This model is commonly considered to require a relatively marked increase of T_g as χ is increased.

Any relatively small shift (if it is in fact greater than zero) of the true value of T_g for PCTFE implied by the \bar{V} - T and mechanical loss data could be at least in part due to liquid orientation effects induced by the crystallization process. However, the small magnitude of the observed shift, 5 °C or less, does not seem consistent with the large shift that one would expect if specimens 0.27(M), 0.42(M), 0.44, and 0.73 possessed crystals constructed principally on the bundlelike pattern. In the chain-folded pattern of crystal growth, the molecular connections between the crystals (interlamellar links)

will ordinarily be much less frequent than the number of intercrystalline links in the bundlelike system.

The above implies that the crystals in the quench crystallized and quench \rightarrow annealed specimens (0.27(M), 0.42(M), 0.44, and 0.73) may be at least partly chain-folded in character. The chain-folded lamellae in such specimens are undoubtedly small in size and somewhat disorganized with respect to their mutual orientation, as compared to the situation in a well-formed lamellar spherulite. The 0.80 specimens contain large and well-formed lamellae with a substantial degree of chain folding.

It is considered to be of interest to comment briefly on what the present data and interpretation for the resolved high and intermediate peaks, and the single "mixed" high and intermediate peak in PCTFE, imply in the case of other polymers. A number of points are brought out that may prove useful in future investigations.

(1) It is clear that degree of crystallinity should not in all cases be expected to describe the specimen fully with respect to the high- and intermediate-temperature peaks. A case in point is the $\chi=0.80$ PCTFE specimen with resolved high and intermediate dielectric peaks, as compared with the $\chi=0.73$ specimen with a single "mixed" peak. Here the difference results ultimately from the different methods used to attain the high crystallinity, the $\chi=0.80$ specimen being typically lamellar spherulitic, and the 0.73 specimen possessing no large crystals. Entirely apart from suggesting that the high-temperature peak is associated with regular lamellar structures, these results suggest one reason why other polymers may in some cases exhibit but one "mixed" peak in the appropriate temperature range, rather than two resolved peaks. The present results on PCTFE show that the quench \rightarrow anneal technique of crystallization leads to a single "mixed" dielectric loss process in the polymer. A similar result may be anticipated in other polymers, if large spherulites do not form during the quenching or annealing process.

The interesting work of Thompson and Woods [20] on nonspherulitic polyethylene terephthalate (PETP) filaments formed by quenching from the melt followed by annealing with crystallization appears to fit in this pattern, since only a single mechanical loss peak is observed. (Unfortunately the mechanical loss of highly spherulitic specimens of PETP crystallized from the melt at low undercooling has apparently not been studied. Such specimens may exhibit resolved high and intermediate peaks.) In contrast, polyethylene usually crystallizes very rapidly on cooling from the melt, rendering it difficult to avoid the formation of lamellar structures in specimens of ordinary size; this polymer commonly exhibits clearly resolved high- and intermediate-temperature loss peaks, as shown by Takayanagi [46]. However, by the use of stringent quenching techniques prior to annealing, Takayanagi has succeeded in suppressing the high-temperature peak in a highly crystalline specimen of polyethylene to the point that only a single

(intermediate) peak is found [18]. These two types of result on polyethylene are highly reminiscent of our results on PCTFE with specimens 0.80 (spherulitic crystallized from melt) and 0.73 (nonspherulitic; quench→annealed).

(2) The appearance of but a single loss peak in the high-intermediate region may in some cases result simply from the fact that very little amorphous material is present in a highly crystalline specimen, causing only the high-temperature peak to appear. This condition was approached but by no means reached with PCTFE in $\chi=0.80$, but was evidently found by Takayanagi and coworkers in a very highly crystalline ($\chi=0.90$ to 0.94) specimen of linear polyethylene (Marlex 50) [17]. Less crystalline polyethylene specimens clearly exhibit both peaks.

(3) The relative insensitivity of T_g and related effects to degree of crystallinity exhibited by PCTFE may not obtain in other polymers, especially if other modes of crystallization are employed. For example, crystallization of highly oriented quenched fibers might lead to substantially more bundlelike character than the other methods. In this case, a single loss peak that shifted markedly with degree of crystallinity may be found which corresponded to a true increase of T_g as measured by the \bar{V} - T method. This may be at least a partial explanation of the large shifts (*circa* 40 °C) observed by Thompson and Woods with extruded filaments of PETP [20].

The dielectric data on PCTFE suggest that caution must be used in predicting true shifts in T_g when the intensity and crystal-size factors involved in "mixing" are the real causes of the shift of the loss maximums. The mechanical analog of this effect could easily arise in some polymers. In any case, the authors believe checking the actual shift of T_g by the \bar{V} - T method is a useful precaution against misinterpretation in such cases.

4.2. Dipolar Polarization and Large High-Frequency Contribution of the Crystals to the Dielectric Properties

One contribution of the crystals (or more likely their surfaces) to the dielectric properties has already been uncovered in PCTFE—the high-temperature mechanism. As will be seen shortly, the actual contribution of this effect to the dielectric constant is quite small. The principal objective of this section is to show that the crystals contribute another and generally much more prominent component to the static dielectric constant which is associated with a relaxation time that is extremely short. It will further be shown that this large high-frequency crystal contribution is a bulk property of the crystals.

It can be shown that the effective contribution of the dipole orientation polarization, $\langle P_\mu \rangle_{\text{eff}}$, to the static dielectric constant is given with sufficient accuracy by the expression

$$\bar{V}(\epsilon_s - \epsilon_\infty) \propto \langle P_\mu \rangle_{\text{eff}} \quad (9)$$

where \bar{V} is the specific volume, ϵ_s the ultra-low-frequency (static) value of ϵ' , and ϵ_∞ the limiting high-frequency value of ϵ' .¹² The quantity ϵ_∞ includes the contribution of electronic and atomic (infrared) polarization. The quantity $(\epsilon_s - \epsilon_\infty)$ is the increment of dielectric constant due to all the observed dipole orientation phenomena.

For the liquid specimen (0.0), ϵ_s was taken as the value of ϵ' as given in table 6, since at the high temperatures employed, about 200 to 250 °C, the relaxation effects occurred at frequencies much higher than were used in the measurements. The value of ϵ_s for the other specimens was obtained by extrapolation of the data on a Cole-Cole plot (ϵ'' versus ϵ') [21] to the abscissa on the low-frequency side of the curve. Some typical Cole-Cole plots are shown in figure 20.

In theory, ϵ_∞ can also be determined by extrapolation of the Cole-Cole plot to the abscissa of the high-frequency side of the curve. In practice however, this method of obtaining ϵ_∞ could be applied with high accuracy only at the lowest temperatures where many points fall close to ϵ_∞ . The values of ϵ_∞ employed at other temperatures were calculated from the most reliable low-temperature value obtained from a Cole-Cole plot ($\epsilon_\infty=2.30$, $T=-50$ °C, specimen 0.44, shown in fig. 20a) using the Gladstone-Dale equation [22].¹³

$$R_{G-D} = \text{constant} = (n-1)\bar{V} = (\sqrt{\epsilon_\infty} - 1)\bar{V}. \quad (10)$$

In using this equation the assumption is made that the atomic or electronic polarizability of a molecular constituent is not seriously affected by whether the constituent lies in the amorphous or the crystalline regions.

The behavior of $\bar{V}(\epsilon_s - \epsilon_\infty)$ as a function of temperature for the various specimens is shown in figure 21. One of the most striking features of figure 21 is the fact that $\bar{V}(\epsilon_s - \epsilon_\infty)$ for specimen 0.80 at 200 °C ($\chi=0.65$) is considerably higher than the 200 °C point on the line showing the typical dipolar liquid behavior of specimen 0.0. This marked increase in $\langle P_\mu \rangle_{\text{eff}}$ above the liquid value when the crystals form in the system near T_m strongly suggests that the crystalline phase makes quite a large contribution to the dipolar polarization. It will be demonstrated shortly that this is correct.

In order to identify at least a major part of this proposed crystal polarization, recall that in figure 2 the 23 °C loss index data of specimen 0.80 gave a strong indication of a loss peak at microwave frequencies. The existence of this peak is also borne out by the data of Hartshorn, Parry, and Rushton [2]. It is this high-frequency loss process that leads

¹² Fröhlich has shown on very general grounds that $\langle P_\mu \rangle_{\text{eff}} = (4\pi N/3) (\overline{mm^2}/kT) = (\epsilon_s - \epsilon_\infty)\bar{V}/f$ where f is the slowly varying function $(2\epsilon_s + \epsilon_\infty)/3\epsilon_s$ [23]. The quantity $\overline{mm^2}$ gives the magnitude of the square of the effective dipole moment resulting from orientation of dipoles, including short range interactions.

¹³ Carr and Zimm [24] found that eq (10) applies more accurately to the estimation of the square of the index of refraction ($\epsilon_\infty = n^2$) as a function of density than the Lorentz-Lorenz, or various other expressions. The results for ϵ_∞ at other temperatures would have differed but little if the Lorentz-Lorenz expression, $[(n^2-1)/(n^2+2)]\bar{V} = R_{L-L}$, had been employed.

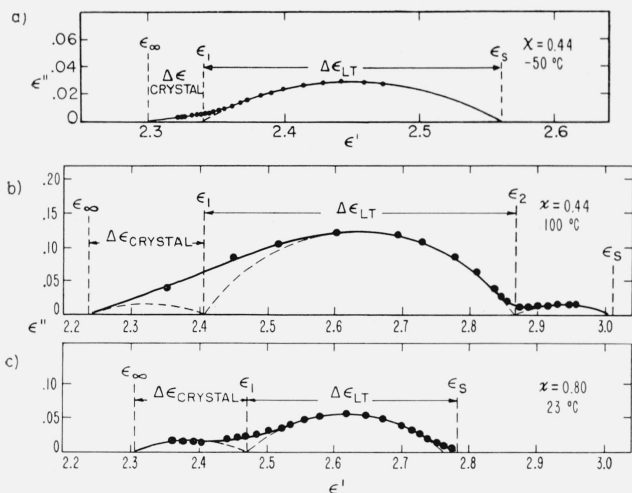


FIGURE 20. Typical Cole-Cole plots of the dielectric data.

to the high-frequency contribution in the room-temperature Cole-Cole plot for specimen 0.80. This contribution is labeled $\Delta\epsilon_{\text{crystal}}$ in figure 20c. (Justification for this identification is given below.) The microwave data are those near $\epsilon' = 2.35$. The magnitude of $\Delta\epsilon_{\text{crystal}}$ was calculated from the Cole-Cole plots for the other specimens at various temperatures as the difference $\epsilon_1 - \epsilon_\infty$ (see fig. 20b). Here ϵ_1 is the value of ϵ' at which a circular arc, which fits the data for the "low-temperature" or the main loss peak over the major part of its range, intercepts the abscissa on the high-frequency side. The value of ϵ_∞ was determined from eq (10). In all cases except the room-temperature data of specimen 0.80, where microwave data revealed the resolved process, $\Delta\epsilon_{\text{crystal}}$ manifested itself simply as a "tail" or asymmetry on the high-frequency side of the main arc. (See data at 100 °C for $\chi = 0.44$ in fig. 20b). $\Delta\epsilon_{\text{crystal}}$ does not include the small crystal contribution of the high-temperature process.

The contribution of $\Delta\epsilon_{\text{crystal}}$ to $\bar{V}(\epsilon_s - \epsilon_\infty)$ obtained in the above manner for the various specimens is shown in figure 22 over the temperature range where the determination is considered reliable. The behavior of $\bar{V}\Delta\epsilon_{\text{crystal}}$ with temperature is in all cases that typical of a crystalline phase which is becoming more disordered with increasing temperature, i.e., $d(\bar{V}\Delta\epsilon_{\text{crystal}})/dT$ is positive. Furthermore, the value of $\bar{V}\Delta\epsilon_{\text{crystal}}$ for any specimen is directly proportional to the degree of crystallinity to within the experimental error. The value of $\bar{V}\Delta\epsilon_{\text{crystal}}$ extrapolated to the pure crystal is also shown in figure 22.

We therefore conclude that the very high-frequency process shown in the 23 °C ϵ'' versus $\log f$ data of figure 2, and which gives rise to $\Delta\epsilon_{\text{crystal}}$ on the Cole-Cole plots, is a bulk crystal property, and further, that the increase in $\bar{V}(\epsilon_s - \epsilon_\infty)$ upon crystallizing a specimen from the melt is due chiefly to the dipole orientation polarization of the crystals formed. The contribution $\bar{V}\Delta\epsilon_{\text{crystal}}$ may not be

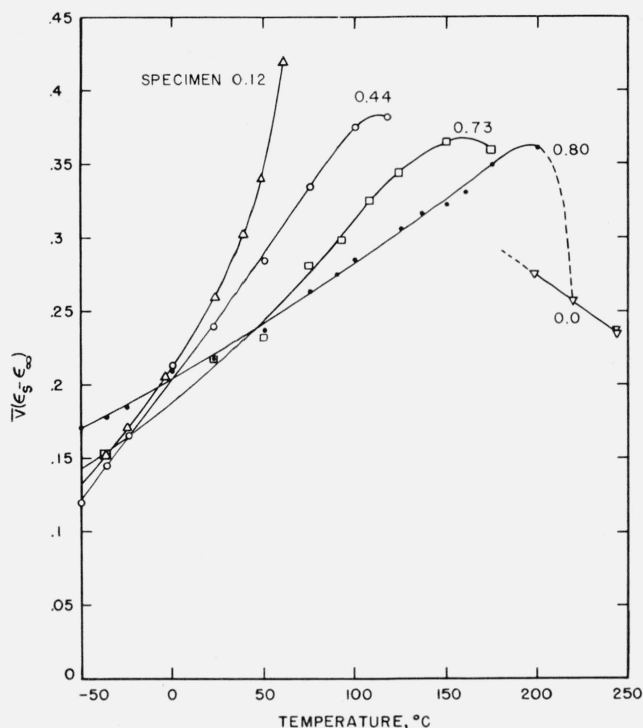


FIGURE 21. The temperature dependence of $\bar{V}(\epsilon_s - \epsilon_\infty) \cong \langle P_\mu \rangle_{\text{eff}}$ for the various specimens.

$\langle P_\mu \rangle_{\text{eff}}$ is nearly proportional to $\bar{V}(\epsilon_s - \epsilon_\infty)$, where \bar{V} is the specific volume in cm^3/g , and $(\epsilon_s - \epsilon_\infty)$ is the increment of dielectric constant due to the total dipolar relaxational polarization.

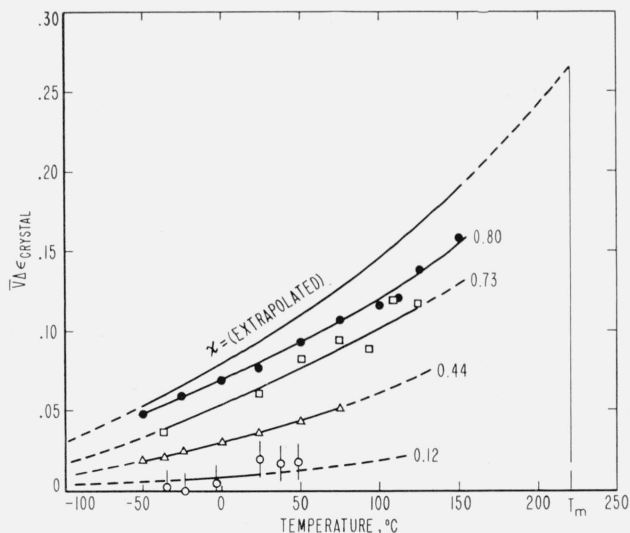


FIGURE 22. $\bar{V}\Delta\epsilon_{\text{crystal}}$ versus the temperature.

The curves indicate that $(\bar{V}\Delta\epsilon_{\text{crystal}})$ is directly proportional to χ , and justifies identifying the corresponding relaxational phenomena as a bulk property of the crystalline phase.

the sole crystal contribution to $\bar{V}(\epsilon_s - \epsilon_\infty)$, but it certainly is by far the largest one at most temperatures.

The work of Reynolds and coworkers [1] on the dielectric properties of low molecular weight PCTFE (mol wt=980) lends support to our finding that the crystals of PCTFE exhibit strong dipolar orientation

polarization and that this crystal polarization leads to a high-frequency "tail" or asymmetry in the data on a Cole-Cole plot. These authors were able to observe a relaxation peak in the pure liquid phase above the crystal melting point of their low molecular weight polymer. On a Cole-Cole plot, these data gave a regular circular arc with no evidence of a high-frequency "tail." Upon cooling the specimen and allowing crystals to form, the value of the static dielectric constant rose to surprisingly high values ($\epsilon_s \approx 8$). Furthermore, the dielectric data taken with the crystals in the system yielded a Cole-Cole plot with a sizeable "tail" or asymmetry on the high-frequency side.

From the standpoint of the ϵ'' versus T plots at 1 c/s, the crystal polarization found above does not lead to a loss peak in the observed temperature range. Its critical frequency even at 23 °C is around 10^{10} c/s, and this critical frequency almost certainly does not fall near 1 c/s even at -50 °C. The crystal relaxation peak on an ϵ'' versus T plot at 1 c/s would probably appear in the general vicinity of -100 °C or below, and be quite small because of the greatly diminished value of $\Delta\epsilon_{\text{crystal}}$ at such low temperatures (see fig. 22).

The crystal polarization process is somewhat unusual in two respects. First, the relaxation time associated with it is extremely short ($\tau \sim 10^{-11}$ sec at 23 °C), indicative of a low free energy of activation, and second, the polarization is rather strong, increasing to a value comparable to that of the normal liquid just below the melting point. Molecular reorientation of simple polar chain molecules about the long molecular axis leading to dielectric polarization and loss is a well known phenomenon [25, 26], but a rotation *en bloc* of large sections of the polymer chain of this type is probably not the sole cause of the high-frequency process in PCTFE. In a rigid single-axis rotator, only the component of the dipole moment perpendicular to the chain axis contributes to the orientation polarization. The chain of PCTFE is believed to possess a spiral twist [27] with a repeat distance of roughly 15 Å. Whether the chain be syndiotactic or isotactic, this structure necessitates that the resultant dipole moment of a long section of chain (regarded as being rigid) would have only a very small component normal to the chain axis due to vectorial cancellation. The "rigid rod" model with spiral twist thus does not seem capable of explaining the high polarization observed, even if free intermolecular rotation about the long axis is assumed. Also, such a model would probably tend to suggest a longer relaxation time than is found experimentally. The latter is especially the case where chain folds exist at the ends of the chain elements. (In PCTFE crystallized at 180 °C the lamellae are roughly 300 Å thick [28].)

One possible explanation of the high polarization and the short relaxation time is that the electric field distorts individual sections of the spirally twisted chain in the crystal, causing a local untwisting that leads to a large local dipole moment which then gives rise to dipolar polarization. The energy and geometry of one particular type of local

uncoiling of a helical chain in a crystal has been considered by Reneker [29] in terms of point defects. He has concluded in the case of the polyoxymethylene chain, which has a spiral twist superimposed on a larger helix, that the local uncoiling of the larger helix would have a low energy of activation (about 2 kcal/mole), since such local uncoiling can be accomplished with only a slight disruption of the surrounding lattice. It is not clear whether this particular type of uncoiling could occur in PCTFE, since a detailed knowledge of the structure is lacking. Nevertheless, some type of local uncoiling or untwisting of the polymer chain seems the best possibility to explain the magnitude and rapidity of the dipolar polarization observed for the crystalline phase. The increase in dipolar polarization with increasing temperature observed in PCTFE is consistent with this suggestion.

If the above proposal is correct, one would expect that other polymers with spirally twisted molecules might exhibit a high-frequency crystal relaxation. For example, crystalline polyoxymethylene may prove to exhibit a high-frequency crystal relaxation process similar to that found in PCTFE in the microwave region.

4.3. The Low-Temperature Relaxation Process

The frequency dependence of the low-temperature relaxation process in specimens of various crystallinities and at various temperatures has been presented in figures 2, 7, 10, and 12. This loss process is from a dielectric standpoint the most prominent in PCTFE, and leads to the large low-temperature peak when the data are plotted on an ϵ'' versus temperature plot as shown in figure 16a.

An estimate of the contribution of this low-temperature process to $\langle P_{\mu} \rangle_{\text{eff}}$ can be established by dealing with the results obtained from the Cole-Cole plots such as those in figure 20. If $\overline{V}\Delta\epsilon_{\text{crystal}}$ (fig. 22) is subtracted from the value of $\overline{V}(\epsilon_s - \epsilon_{\infty})$ (fig. 21) for each of the specimens, the curves shown in figure 23a are obtained. These curves represent the sum of the contributions of the low-, intermediate-, and high-temperature processes to $\langle P_{\mu} \rangle_{\text{eff}}$. The dashed line marked " $\chi=0$ extrapolated" represents an estimate of the behavior of the pure normal amorphous phase. This is based both upon an extrapolation of the high-temperature pure liquid points, and the curve for specimen 0.12 at lower temperatures. The behavior of the hypothetical pure amorphous phase of PCTFE depicted by this dashed line features a maximum between 50 and 100 °C which is readily apparent even in the 0.44 (56 percent amorphous) specimen. (It should be recalled that direct measurement of the dielectric properties of a completely amorphous specimen would be impossible between about 50 and 200 °C because rapid crystallization would occur).

If from the Cole-Cole plots one estimates the magnitude of the contribution of the high- and intermediate-temperature processes to $\overline{V}(\epsilon_s - \epsilon_{\infty})$ and subtracts this contribution (shown in fig. 23b) from

the appropriate curves of figure 23a, then one obtains the curves shown in figure 23c.

The curves in figure 23c represent the contribution, $\bar{V}\Delta\epsilon_{LT}$, of the low-temperature process in the various specimens to $\langle P_{\mu} \rangle_{\text{eff}}$. The $\chi=0$ dashed line represents our best estimate of the contribution of the low-temperature process in the pure normal amorphous phase to $\langle P_{\mu} \rangle_{\text{eff}}$. At low temperatures, this line is based on a simple extrapolation of the $\chi=0.12$ data. The general appearance of the $\chi=0$ line in figure 23c between -50 and $+150$ °C leaves little doubt that a totally amorphous specimen of PCTFE would exhibit a prominent low-temperature process effect. The $\chi=0.44$, $\chi=0.12$, and $\chi=0$ (extrapolated) lines clearly indicate that some type of dielectrically active molecular motions exist in the amorphous phase of the polymer far below the ordinary glass transition at $T_g=52$ °C.

The line indicated as $\chi=1$ (extrapolated) in figure 23c will be discussed subsequently.

Further evidence can be cited that shows that the amorphous phase makes a large contribution to the low-temperature effect. The low-temperature process gives rise to the main broad arc of width $\Delta\epsilon_{LT}$ when the dielectric data are placed on a Cole-Cole plot, as shown in figure 20. As mentioned earlier, Reynolds and coworkers [1] obtained similar Cole-Cole plots of their data on low molecular weight PCTFE waxes. Their work supports our belief that the amorphous phase makes a large contribution to the low-temperature process. Their Cole-Cole plot for the pure liquid phase consists of a simple arc. The arc component persists also in their semicrystalline specimens measured at lower temperatures. Furthermore, their $\log f_m$ versus $1/T$ plot (derived from the loss peaks which gives rise to the arc in the Cole-Cole plot for the semicrystalline specimen) gives a straight line that passes through the point obtained from the loss data of the pure liquid above the melting point. This demonstrates that the low-temperature process is controlled chiefly by molecular motions in the amorphous phase of low molecular weight PCTFE. The apparent heat of activation of the relaxation process they observed was 19 kcal/mole, which is quite similar to the value of 17.4 kcal/mole obtained by us for the low-temperature process as extrapolated to $\chi=0$ (see below).¹⁴

a. Effect of Crystallization on the Low-Temperature Process. Anomalous Behavior at High Crystallinity

The principal seat of the low-temperature process in moderate or weakly crystalline specimens has been clearly established above as the amorphous component. The objective of this section is to indicate the nature of the complications introduced into the low-temperature effect by high crystallinity.

One manifestation of the effect of crystallinity on the low-temperature process is a large shift of the

¹⁴ Reynolds and coworkers tentatively associated the arc portion of the Cole-Cole plots to the crystals, but we believe the revised interpretation given above is the correct one. There is however, agreement on the general fact that the crystals contribute to the dipolar polarization.

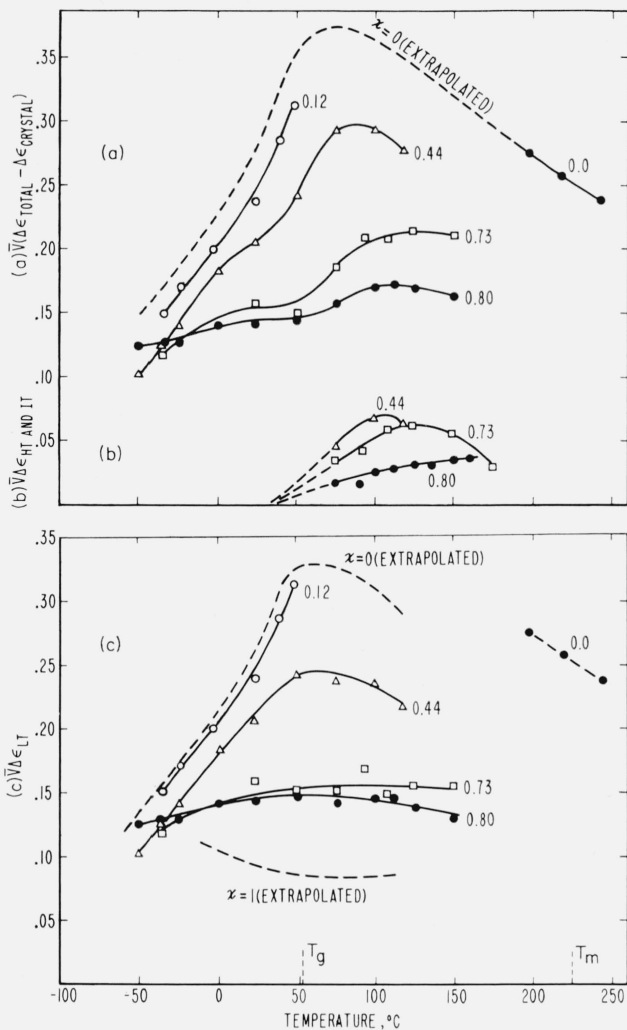


FIGURE 23. Resolution of the components of the dipolar contributions to $\bar{V}(\epsilon_s - \epsilon_\infty) \simeq \langle P_{\mu} \rangle_{\text{eff}}$.

- The total value $\bar{V}(\epsilon_s - \epsilon_\infty)$ less the crystal contribution, $\bar{V}\Delta\epsilon_{\text{CRYSTAL}}$.
- The contribution of the high- and intermediate-temperature processes to $\bar{V}(\epsilon_s - \epsilon_\infty)$.
- The contribution of the low-temperature processes to $\bar{V}(\epsilon_s - \epsilon_\infty)$.

maximums with χ in the $\pi \tan \delta$ (mechanical) and ϵ'' (dielectric) versus T plots shown in figure 16. The temperature of the maximum, T_{max} , of the low-temperature process at 1 c/s is given in table 9 as a function of χ . It is seen that there is a close correspondence between T_{max} in the dielectric and mechanical cases, and that T_{max} falls as χ increases. By a simple extrapolation, it is readily estimated that T_{max} is -10 °C for $\chi \rightarrow 0$ and -45 °C for $\chi \rightarrow 1$.

Correspondingly, figure 17 shows that in the temperature interval from 0 to $+50$ °C the frequency of the maximum of the low-temperature process, at constant temperature, increases as χ increases.¹⁵ Mikhailov [3] has observed a similar shift.

¹⁵ In figure 17 the small change of slope in the $\log f_m$ versus $1/T$ plot of the low-temperature process near 50 °C is probably attributable to secondary effects connected with the glass transition. Above 75 °C, however, the maximum lies in the more inaccurate Q -meter measurement range so that the apparent change in slope could possibly arise from error in locating f_m .

TABLE 9. Temperature at the loss maximum of the low-temperature process observed by dielectric and mechanical methods at 1 c/s

χ	T_{max}	
	Dielectric	Mechanical
0.12	-13 ± 5 °C	-----
.27	-----	-18 ± 5 °C
.42	-----	-30 ± 5 °C
.44	-30 ± 5 °C	-----
.80	-41 ± 5 °C	-40 ± 5 °C

The activation energy for the low-temperature dielectric process shows a slight dependence of χ , as indicated in table 8. The activation energy is larger for the case $\chi \rightarrow 0$ ($\Delta H^* = 17.4$ kcal/mole) than for the case $\chi \rightarrow 1$ ($\Delta H^* = 13.5$ kcal/mole).

Perhaps the most obvious manifestation of the effect of crystallinity on the low-temperature process is the excess polarization denoted by the dashed line marked $\chi=1$ (extrapolated) in figure 23(c). The implication is that the abnormality resides mostly in the highly crystalline specimens. The fact that $\chi=1$ (extrapolated line) is well above the abscissa is not a result of an accumulation of experimental errors. In figure 24, it is readily apparent that the high-frequency crystal relaxation is widely separated from the main loss peak at 23 °C. The area under the main loss peak in figure 24 (as extrapolated to $\chi=1$) leads to the anomalous contribution to $\bar{V}\Delta\epsilon_{LT}$

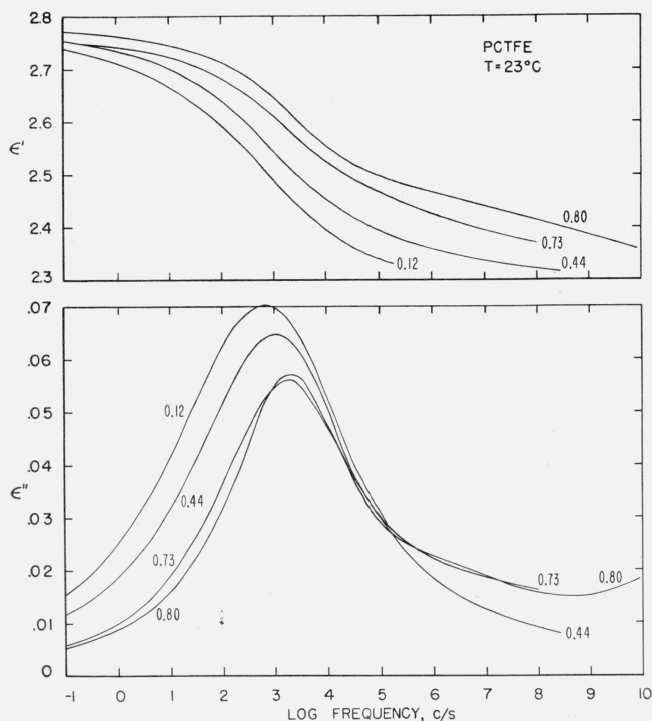


FIGURE 24. Comparison of ϵ'' and ϵ' versus frequency curves at 23 °C for specimens of different crystallinities.

The large loss peak near 10^3 c/s is due to the low-temperature mechanism. The contribution near 10^{10} c/s is due to the high-frequency crystal mechanism.

at $\chi=1$ (extrapolated) shown in figure 23c.¹⁶ It follows that the high-frequency crystal relaxation process is *not* responsible for the anomalous contribution to the low-temperature process at high χ .

It is of importance to indicate that a similar anomaly does not occur, at least in such pronounced form, in all semicrystalline polymers. In a similar analysis of the low-temperature process in polyvinyl alcohol (PVA), Ishida, Takada, and Takayanagi [30] found that $\epsilon_s - \epsilon_\infty$ depended linearly on the fraction of amorphous material between $\chi=0.37$ and 0.58, and extrapolated to zero for $\chi \rightarrow 1$. This crystalline polymer is atactic, and the dipoles in the extended chain configuration are not spirally arranged about the carbon chain axis as in PCTFE.

No completely satisfactory explanation of the origin of the anomalous contribution to $\bar{V}\Delta\epsilon_{LT}$ at high χ in PCTFE has been found. It could be due to a heretofore hidden contribution of the crystals. If so, the crystals would have to be highly disordered, and give a contribution to $\bar{V}\Delta\epsilon_{LT}$ that is nonlinear with χ . Conceivably, the crystal phase involved may be a bundlelike (non-folded) one, consisting of shorter chains segregated out as the chain-folded lamellae form from the longer molecules. Alternatively, the anomalous contribution of $\bar{V}\Delta\epsilon_{LT}$ for $\chi \rightarrow 1$ may be an abnormality induced into the amorphous phase by the presence of a large fraction of lamellar crystals. The present data are incapable of clearly indicating which, if any, of these explanations is correct.

None of the interesting peculiarities exhibited by the highly crystalline PCTFE specimens at low temperatures detract from the concept that the low-temperature process in its unperturbed form is basically a property of the amorphous component of the polymer.

b. Nature of the Molecular Mechanism

The overall heat of activation, ΔH^* , of the low-temperature process, according to table 8, centers around 15.6 kcal/mole. For the case $\chi \rightarrow 0$, it is 17.4 kcal/mole. Furthermore, this value is essentially independent of temperature. Both the low value of ΔH^* and its insensitivity to temperature indicate that the responsible molecular motion corresponds to dipole orientation over a fairly simple barrier system. It seems clear that only a relatively small number of chain segments can be directly involved. A kinking or "jump rope" motion in the amorphous phase involving but a few chain segments would suffice to explain the effects noted experimentally. The activation barrier that the dipoles involved must surmount in order to orient would in this case originate partly from hindered rotation in the chain itself, and partly from hindrances due to nearest neighbors. The large contribution to $\langle P_\mu \rangle_{eff}$ by the low-temperature mechanism is consistent with the proposed type of motion in a molecule with dipoles rigidly attached at a right angle to the main chain backbone.

¹⁶ The mechanical loss data in figure 16 also indicate that extrapolation to $\chi=1$ will not remove the low-temperature peak.

The observation that the low-temperature process in PCTFE is mainly a result of motions in the amorphous (glassy) phase is especially significant in view of the fact that it shows that rapid molecular motions persist far below the usual glass transition at $T_g=52^\circ\text{C}$. This cannot possibly be ascribed to independently rotatable side groups in the case of PCTFE. The results obtained here clearly imply that the purely amorphous phase of a polymer with dipoles rigidly attached at a right angle to the main chain backbone exhibit a bimodal set of relaxation times. The long set "freezes out" at 1 c/s above T_g and must involve complex long-range motions of sizeable parts of the molecules (intermediate-temperature process). The shorter set freezes out far below T_g at 1 c/s, and corresponds to a simpler motion involving a much smaller number of chain segments (low-temperature process). These two relaxation processes (or loss peaks) themselves are not properly termed "transitions," and we have avoided this usage. However, some type of transition may underlie one or both of the relaxation effects.

The intermediate-temperature process foretells the transition supercooled liquid \rightarrow glassy state at $T_g=52^\circ\text{C}$. In some respects, the low-temperature process in a largely amorphous specimen may be regarded as denoting the onset of a "transition" within the glassy state. However, it is not known from the present work whether the "freezing out" of the low-temperature process would lead to a break in the $\bar{V}-T$ curve similar in general character to that at $T_g=52^\circ\text{C}$ associated with the intermediate-temperature process. Extrapolation of the log f_m versus $1/T$ plot for specimen 0.12 (fig. 17) to 0.01 c/s gives $T=-60^\circ\text{C}$. Interestingly, Bacca-redda and Butta [31] have found a break in their sound velocity versus temperature data on PCTFE at -58°C (as well as at $+48^\circ\text{C}$) in a 51 percent crystalline specimen. Such breaks in sound-velocity data often occur at the same temperature as breaks in $\bar{V}-T$ data or specific heat data.

4.4. Maxwell-Wagner Polarization

Before giving the summary of the interpretation, it will be shown that none of the relaxation effects observed were due to Maxwell-Wagner polarization.

Reynolds and coworkers [1] suggested that since semicrystalline PCTFE consists of a two-phase system, some of the observed relaxation effects may have resulted from Maxwell-Wagner polarization. Nakajima and Saito [6] rejected this mechanism on the grounds that the observed d-c conductivity of neither phase is large enough to give any effect in their measurement region. Since the present work extends the measurements on the two phase system up to 200°C , where higher d-c conductivities were observed, it is necessary to reinspect the problem.

Since the resistivity increases as the specimen is crystallized, we shall regard the crystals as non-conducting regions imbedded in a semiconducting

matrix—the amorphous phase. We shall apply the equations developed by Wagner [32] to describe the dielectric properties of a composition consisting of a low concentration of spheres of one material dispersed through a matrix of another material. Wagner's equation is applied despite the facts that (a) we have no assurance that the crystals are spherical and, as is pointed out by Sillars [33], the crystal shape can alter the results appreciably, (b) we are extending it to a much higher concentration of spheres than Wagner visualized. Wagner's equation predicts a Debye-type loss peak (after the d-c conductivity effect is subtracted out). The peak has a relaxation time τ and an associated change in dielectric constant $\Delta\epsilon$ given by

$$\tau = \frac{3\epsilon_0\epsilon'\rho}{(2+q)} \quad (11)$$

and

$$\Delta\epsilon = \frac{3q(1-q)\epsilon'}{(2+q)^2} \quad (12)$$

Here ϵ' is assumed to be nearly the same for the two phases, ρ is the resistivity of the amorphous matrix in ohm-cm, q is the volume fraction of crystals ($q \cong \chi$). From the observed resistivity of the specimen, ρ_s , the resistivity of the matrix, ρ , can be computed from the equation [32],¹⁷

$$\rho = \rho_s \frac{2(1-q)}{2+q} \quad (13)$$

At 200°C , ρ_s for specimen 0.80 was 7×10^{15} ohm-cm. Therefore, ρ is about 2.5×10^{15} ohm-cm. Substituting into eqs (11) and (12) we find $\tau=760$ sec and $\Delta\epsilon=0.3$. A Debye-type loss peak is therefore predicted at a frequency of about 2×10^{-4} c/s, with a peak height of 0.15. A relaxation process of this nature would not detectably affect the data even at 0.1 c/s. Therefore, Maxwell-Wagner polarization is not responsible for the relaxation processes occurring at higher frequencies or at lower temperatures. In only one case was an appreciable conductivity effect noted in a crystalline specimen after the measured d-c contribution to ϵ'' had been subtracted. In the 175 and 200°C data for specimen 0.80 shown in figure 6, a large upswing is seen in ϵ'' at the lowest frequencies. This was identified as being principally a conductivity effect and was not taken as indicating a true relaxation mechanism. In any event, this conductivity does not lead, through the Maxwell-Wagner effect, to the loss peaks at higher frequencies shown in figure 6.

If the crystals are assumed to be ellipsoids with a high axial ratio (corresponding electrically to individual lamellae) the proposed Maxwell-Wagner effect would occur at a frequency still lower than that calculated using the spherical approximation.

Equation (11) shows that τ is proportional to ρ , the resistivity of the amorphous matrix. In this connection, it is of interest to note that the resistivity of a specimen decreases considerably while the

¹⁷ The applicability of the equation $\rho = \rho_s(2+q)/(2-2q)$ to the present situation was roughly checked. Crystallizing a specimen of PCTFE at 200°C to a degree of crystallinity near 0.57 resulted in an increase in the resistivity to 2.7 times the value of the liquid ($\rho_s=(2.7)\rho$). Equation (13) with $q=0.57$, predicts $\rho_s=(2.99)\rho$, which is in reasonable agreement with the experimental observation.

specimen is maintained near or above 200 °C. If thermal degradation (or indeed any other mechanism) reduces the resistivity sufficiently, the predicted Maxwell-Wagner peak will move sufficiently far into the measurable frequency spectrum to combine with or mask the true relaxation peaks. This did not occur in the present study.

4.5. Summary of Interpretation

In the main, the high-, intermediate-, and low-temperature processes uncovered in PCTFE are consistent with an emerging pattern of the dielectric and mechanical behavior of semicrystalline polymers whose chains possess no independently rotatable side groups. A summary giving the important results concerning these mechanisms is given in table 10.

It is useful at this point to mention the nomenclature used by certain other authors in dealing with the specific mechanisms and phases involved in these three effects. Takayanagi calls the resolved high-temperature process in polyethylene, polyoxymethylene, and isotactic polypropylene " α_c ," and attributes it to the effect of chain-folded lamellar structures [17, 18] as we have shown in the case of PCTFE. The resolved intermediate temperature process in the same polymers is denoted " α_a " by Takayanagi, and attributed to relaxations in the amorphous phase, as shown here for PCTFE. The present work on PCTFE establishes a clear relation between the relaxation effects associated with the intermediate-temperature process and the $\bar{V}-T$ glass transition at $T_g=52$ °C. The low-temperature process is called the " β " process in comparable polymers by Takayanagi. The present work shows that it is principally a result of the amorphous phase in PCTFE. On no account should the low-temperature process in the amorphous phase of the type of polymers mentioned above, which have no independently rotatable side groups, be confused with the relaxation effect that occurs in the amorphous phase of polymers that possess independently rotatable side groups, such as poly(methyl methacrylate). This latter effect is also often called " β " [34, 35], but is to be distinguished from the " β " process in polymers without rotatable side groups.

The present work on PCTFE provides insight into the circumstances that allow the intermediate and high temperature processes to appear as two resolved peaks on the one hand, and as one "mixed" peak on the other. Two resolved dielectric loss peaks appear in specimens of high χ crystallized from the melt that contain well-formed lamellar spherulites; a single "mixed" dielectric peak appears in an equally crystalline specimen crystallized without large well-formed spherulites prepared by the quench→anneal technique. Another interesting point clearly brought out by the work on PCTFE is that increasing the degree of crystallinity does not actually lead to a large true increase of T_g as measured by the $\bar{V}-T$ method or by mechanical loss measurements. The apparent increase of T_g implied by the dielectric data is a result of mixing and in-

TABLE 10. Summary of results of analysis of dipolar relaxation and polarization effects in semicrystalline PCTFE

Process	T_{max} for 1 c/s loss peak on ϵ'' versus T plot	Phase involved	Remarks
High-temperature	+150 °C	Chain-folded lamellar crystalline	Appears in resolved form only in highly crystalline spherulitic specimens. $\Delta H^* \approx 80$ kcal/mole. Probably involves lamellar surfaces or interlamellar interactions.
Intermediate-temperature	+95 °C	Normal amorphous	Relaxation effect associated with onset of normal glass transition at $T_g=52$ °C. ΔH^* follows WLF relation with $T_g=52$ °C. Mechanism involves complex motions of many chain segments in amorphous regions.
Low-temperature (normal component)	-10 °C (extrapolated to $\chi=0$)	Normal amorphous	Relaxation effect in amorphous phase associated with short-range reorientation of a few chain segments over fairly simple barrier system (kinking or "jump rope" type motions). $\Delta H^*=17.4$ kcal/mole. Leads to most prominent loss peak observed.
Low-temperature (abnormal component)	-45 °C (extrapolated to $\chi=1$)	Abnormal amorphous or disordered crystal	Appears most prominently in highly crystalline specimens, mixes with normal component. $\Delta H^*=13.5$ kcal/mole. A high degree of orientational disorder is indicated.
High-frequency crystal polarization	Not observed at 1 c/s in temperature range studied. May appear below -50 °C	Crystalline	Bulk property of crystals. Relaxation time very short ($\tau \sim 10^{-11}$ sec at 23 °C). Mechanism may involve untwisting of spiral chain structure. Polarization increases with temperature, becomes comparable to liquid polarization near T_m . ΔH^* unknown, but probably small.

tensity factors. There is no reason to suppose that a phase clearly identifiable as basically amorphous does not exist in semicrystalline specimens of PCTFE even at high χ .

The fact that dielectrically active relaxation effects are observed both above and below the nominal glass transition temperature in the amorphous phase implies that a flexible right-angle dipole polymer liquid (with no independently rotatable side groups) can possess a bimodal distribution of relaxation times. The longer time set "freezes out," near or above T_g , depending upon the frequency, and consists of complex modes of relaxation involving a large number of polymer segments. The shorter time set involves more simple and localized motions which persist at temperatures far below $T_g=52$ °C in the case of PCTFE.¹⁸

An interesting and unusual feature of the present work on PCTFE is the proof of the existence and description of a large bulk crystal polarization effect associated with a very fast dipolar reorientation process. The loss process is so rapid that the corresponding maximum on an ϵ'' versus $\log f$ plot is not quite reached even at 8.6 kMc/s at 23 °C.

¹⁸ If the side group constituting the right-angle dipole rigidly attached to the main chain backbone is large, the simple localized motion leading to the low-temperature process may be subdued or moved to higher temperatures. In such a case, the low-temperature process and the intermediate-temperature process might merge and become indistinguishable. However, this did not occur in PCTFE or the other semicrystalline polymers mentioned above.

This process may appear in other semicrystalline polymers in the microwave region. No large loss peak on an ϵ'' versus T plot at a fixed frequency due to this process was uncovered.

Maxwell-Wagner polarization is incapable of causing any of the loss peaks discussed.

5. Appendix. Micrometer Specimen Holder, Measurement Techniques, and Accuracy of Results for 0.01 c/s to 10 Mc/s

5.1. Introduction

During the course of our investigation of the dielectric properties of PCTFE and other polymeric materials, a number of problems relating to apparatus and measurement techniques were encountered and solved. Doubtless many of these problems were noted and adequately dealt with in various ways by other investigators, but the fact remains that such useful details are rarely published. The object of appendixes 5, 6, and 7 is to give an account of the experimental details in a form that will provide maximum usefulness to workers dealing with other systems, and which at the same time deals specifically with the measurements on the PCTFE specimens used in this research.

In this appendix, the following items are covered:

(a) The construction of the micrometer specimen holder used to make dielectric measurements on rigid disk specimens between 0.01 c/s to 10 Mc/s, and at temperatures ranging from -40 to $+500$ °C. (Descriptions of the two bridges and the Q -meter used with this specimen holder are given in appendix 6.)

(b) Methods used to compute ϵ' and ϵ'' for rigid disk specimens, such as PCTFE 0.80, 0.73, and 0.44, in the micrometer specimen holder.

(c) Analysis of accuracy of results on rigid disk specimens.

(d) Addition of a guard ring to the specimen holder, and the use of this device to measure ϵ' and ϵ'' for deformable materials such as the liquid specimen of PCTFE, 0.0. Also given are details of the experimental procedure, methods of calculation of results, and an analysis of the accuracy.

(e) Modifications of technique used to obtain ϵ' and ϵ'' for thin films (such as PCTFE 0.12) with the micrometer holder. Included here is a special analysis of the effect of surface irregularities in the film, and the effect of surface electrodes.

5.2. Micrometer Specimen Holder

a. Design Requirements

Most of the electrical measurements were made using a two-terminal sample holder which had been designed for use at temperatures from about -40 to $+500$ °C.¹⁹ The substitution method was employed. The holder was designed so that it would have the following features: (a) Low differential thermal expansion so that there is a minimum of warping in the holder, and so that the spacing be-

tween the electrodes can be readily measured at all temperatures. (b) Low dielectric loss in the holder at all temperatures. (c) A means of controlling and accurately measuring the spacing between the electrodes. (d) A means of reproducibly connecting and disconnecting the holder from the two-terminal measuring circuit. (e) Series resistance and inductance should be sufficiently low that the holder may be reliably operated up to 10 Mc/s. A slight modification described later by which the holder may be operated in a three-terminal manner makes it possible to extend the frequency at the lower end to 0.01 c/s using a three-terminal low-frequency bridge [5].

b. Description of Holder

The holder was designed according to the principles given by Hartshorn [36], which eliminate the edge capacitance from the determination of capacitance, and which is a modification of the holder described by Baker [37]. The design is such that the electrodes can be placed in a furnace with controls for separating the electrodes and measuring the spacing between them outside the heated space. A view of this holder is given in figure 25. A schematic diagram of the holder is given in figure 26.

The upper electrode, **C**, is attached to a movable frame consisting of three metal rods, a ceramic disk at the top, and two brass plates, all clamped together to form a rigid framework. This framework moves only in a vertical direction guided by six guide wheels, **O**, which can also be adjusted to center the two electrodes. The wheels are attached to a fixed framework of rods and clamping plates. This fixed framework is rigidly attached to the supporting transite plate, **F**, and supports the silver base plate, **E**. The vertical position of the movable frame and electrode is controlled by the thumb nut, **K**. The position of the movable frame and electrode with respect to the fixed framework is measured by a micrometer screw, **L**. A pulley and counterweight system has been installed (not shown) which reduces the compressive force which the movable upper electrode and framework apply to the specimen when resting on it.

The movable electrode is electrically connected by a silver wire to the silver base plate, **E**, and thus to the stainless steel tube which forms the grounded terminal of the holder. For three-terminal operation with the low-frequency bridge this wire is disconnected from the movable electrode. Electrical contact between the electrode and the appropriate terminal of the low-frequency bridge [5] is established by plunging a brass rod tipped with a phosphor-bronze spring contactor downward through the oven into the hole in the upper electrode ordinarily containing a thermocouple. Electrical insulation between the upper movable electrode and ground is provided by the ceramic disk supporting the electrode. For operation at temperatures above 150 °C it was found desirable to place thin mica washers between all metal to ceramic contacts in order to increase the resistance to ground from the movable electrode.

The lower electrode, **D**, is mounted on a rod, **M**, that is held concentric with the thin-walled tube

¹⁹ The design and construction of this holder was performed as a part of the research project on high-temperature-resistant polymers sponsored by the Ordnance Corps, Department of the Army.

which is welded to the silver base plate, **E**. The rod is axially centered and insulated by two Teflon disks ²⁰ (see **P**, fig. 27). Vertical support is provided through three small fused silica rods, **U**, which pass through the upper Teflon disk. The rod and tube serve as terminals for the holder, and connection is made to the measuring instruments by means of rigid concentric leads, **J**. The silver cover, **B**, is

²⁰ Polytetrafluoroethylene, a product of E. I. DuPont de Nemours Co., Inc.

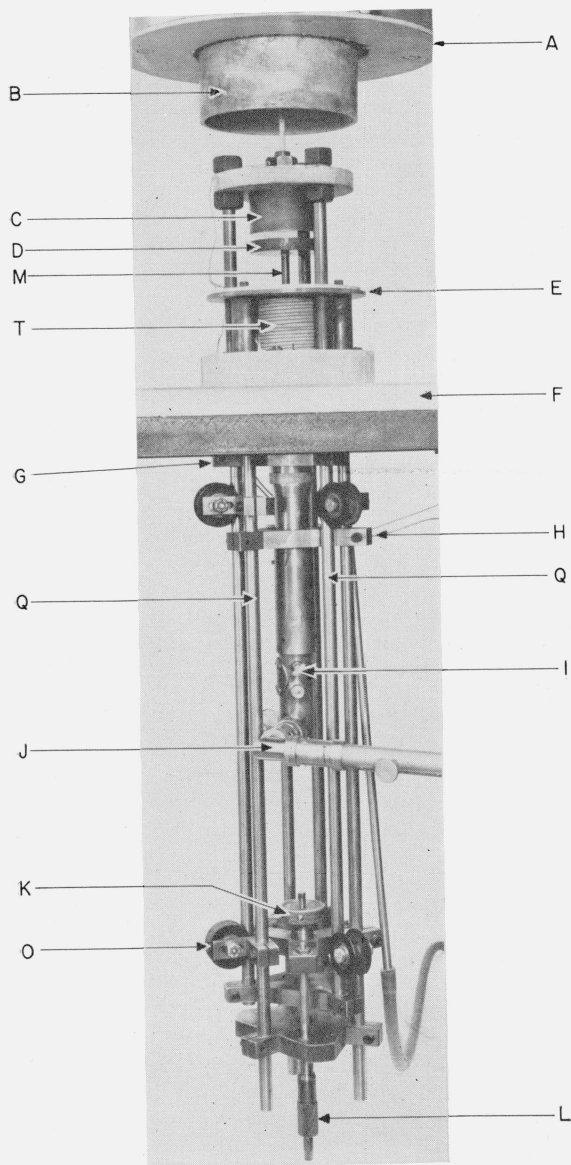


FIGURE 25. Photograph of the specimen holder with the oven, **A**, and the silver cover, **B**, raised.

- A = Cylindrical oven
- B = Silver cover of holder case
- C = Movable electrode
- D = Fixed, insulated electrode
- E = Silver base of holder case
- F = Transite support and base for oven
- G = Clamping plate for movable frame
- H = Clamping plate for fixed frame
- I = Switch
- J = Coaxial leads
- K = Nut for supporting movable frame

lowered over the electrodes to form a complete electrostatic shield. Its high thermal conductivity helps to maintain uniform temperature in the holder.

Low differential expansion was obtained by constructing from the same material all members exposed to heat whose expansion contributes to vertical motion of the electrodes. Thus, the vertical rods, electrodes, and thin-walled tube are made from stainless steel. Stainless steel has a relatively low thermal conductivity, which is a desirable feature in

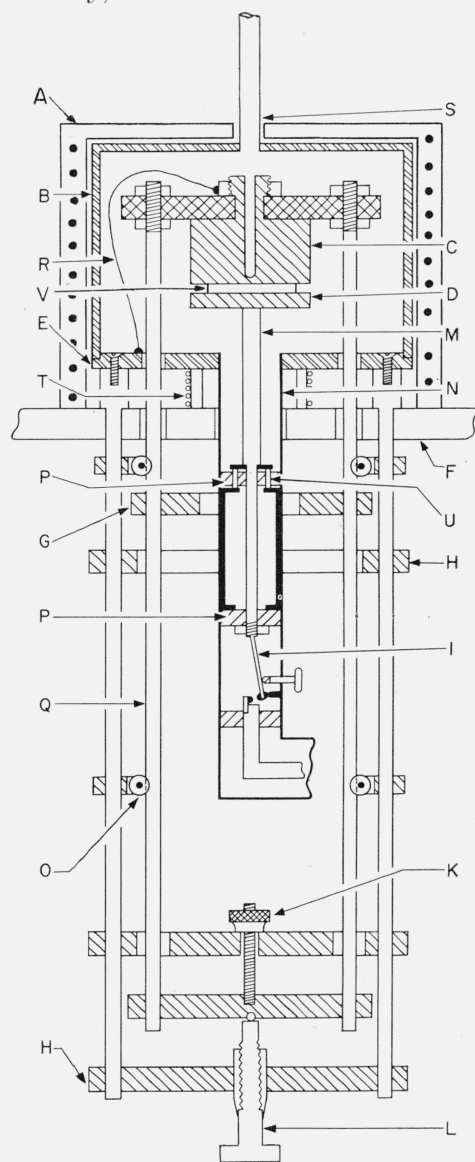


FIGURE 26. Schematic of the specimen holder (not drawn to scale).

- L = Micrometer screw
- M = Support rod for insulated electrode
- N = Thin-walled tubing
- O = Guide wheel
- P = Teflon support washers
- Q = Rod of movable frame
- R = Flexible silver wire
- S = Small tube to permit insertion of thermocouple
- T = Heater coils
- U = Fused silica rods
- V = Disk specimen in measuring position

those parts of the holder which extend outside the electrode area. The differential expansion was determined by noting the micrometer reading at each temperature with the electrodes together. These values were used as corrections to the micrometer "zero" at the appropriate temperature. A further correction was made to compensate for the expansion of the segment of support rod which enters the heated area when the electrodes are separated.

Expansion of the movable framework perpendicular to the axis of the electrodes was nearly eliminated by making the top plate of the movable framework from Stupalith²¹ ceramic, which had a very low coefficient of thermal expansion. The other horizontal plates of the movable framework are outside the heated space. As a result, the warping of the holder is negligible.

Spring washers were placed on the underside of the Stupalith disk so that it was firmly pressed against the upper nut of each of the vertical rods, regardless of the difference in expansion between the rods and the Stupalith. The shoulder of the upper electrode which was pressed against the Stupalith disk, was made large in order to seat the movable electrode firmly to the disk.

Low dielectric loss in the holder was achieved by using Teflon disks to insulate the high-potential electrode, and locating the disks outside of the oven. Because of thermal conduction in the tube and the rod, **M**, the upper insulating disk becomes heated to a temperature approaching 200 °C when the oven is at 500 °C. The electrical properties of Teflon remain sufficiently constant up to this temperature so that the heating of the Teflon disk had no effect on the operation of the holder. At 1 kc/s, over the entire temperature range, this holder has a loss tangent lower than the two-terminal variable air capacitor in the Schering bridge.

For operation above room temperature, heat is supplied by the oven, **A**, and the auxiliary heater, **T**. The auxiliary heater **T** is wound on a ceramic tube about 2 in. in diameter. A thermocouple attached to the silver base plate, **E**, is the sensing element to control the current in the auxiliary heater **T**. After some experimentation, the correct settings of the control temperature and of the currents in the two heaters can be determined such that thermal gradients anywhere in the specimen do not exceed 0.3 °C at any temperature up to 500 °C.

The temperature of the specimen is measured by a thermocouple located at the bottom of a hole drilled down the center of the upper electrode to within 1 mm of the lower surface. The thermocouple is inserted through the top of the oven, **A**, into this hole. The porcelain tube containing the thermocouple can be seen in figure 25 extending out of the hole.

A refrigerated head (not shown) replaces the oven, **A**, for operation down to about -40 °C. (By packing dry ice around the silver can, **B**, lower temperatures can be achieved, but the temperature control problem is then somewhat troublesome.) Tempera-

tures between -40 and 0 °C are attained by supplying heat through a disk-shaped heater element (not shown) which rests on top of the silver can, **B**. A control thermocouple is also located in **B** near this heater. A flow of dried nitrogen gas is maintained in the holder to prevent the condensation of moisture at low temperatures, and to inhibit oxidation at all temperatures.

To assure accurate capacitance measurements using the substitution technique, a switch, **I**, was placed in the coaxial line. This switch consists of a spring contact, attached to the lower end of the rod, **M**. The spring switch is so constructed that its movable end is normally in contact with a grounded adjustable screw, projecting from the tubular shield. The switch is operated by a thumb screw having a Teflon tip which pushes the spring into contact with the center lead. The "open" and "closed" positions of the spring are fixed and highly reproducible thus assuring negligible error in the capacitance determination.

Though it was unnecessary in the present investigation, the stainless steel electrodes were electroplated to prevent their oxidation when operating in air near 500 °C. (Such oxidation would introduce a resistance in series with the specimen.) Gold plated over nickel appeared to be excellent, but with continued use at the high temperatures, the gold color slowly disappeared. The surface remained sufficiently conducting, however, so that no appreciable errors were introduced.

The opposing surfaces of the electrodes were lapped optically flat to within a few wavelengths of light before they were plated. After being plated they were again lapped to remove the unevenness of the plating. After assembly, the surfaces of the electrodes were made parallel by adjusting the nuts above and below the Stupalith disk.

Modification of this holder to incorporate a guard ring is discussed in appendix 5.3a.

c. Preparation of Disk Specimens for Measurement

Specimen stock was carefully selected to be free of foreign matter and voids. After determination of the radius r and thickness t of the disk specimens, they were carefully wiped, and cleaned if necessary. Care was taken to use no materials in cleaning which sorbed into the specimens. (In the case of PCTFE, warm water with detergent was found entirely satisfactory.) After rinsing and thoroughly drying, evaporated gold electrodes were applied *in vacuo*. Enough gold was applied (sometimes in several stages) to give an edge-to-edge resistance of less than 0.2 ohm as measured with point contacts. This assured that resistance effects due to the gold coatings would not affect the loss measurements even up to 10 Mc/s. Such evaporated gold electrodes adhered well to the specimens. The specimens were always flat enough so that very numerous contacts between the electrodes and the gold specimen coating were assured when the specimen was in the holder.

The position of the disk specimen, **V**, in the micrometer holder is shown in figure 26. The specimen radius is kept less than the electrode radius by

²¹ Stupalith 2417, a product of Stupakoff Ceramic Manufacturing Co.

an amount $2t$, so that the edge capacitance will be unaffected by the presence of the specimen, and to assure that the specimen is in the uniform field region.

d. Method of Computing the Dielectric Constant and Loss Index (Disk Specimens)

In all measurements of the dielectric constant of PCTFE specimens 0.80, 0.44, and 0.73 using this holder, the following method was used to calculate ϵ' from the capacitance measurement. (The procedures used for specimen 0.12 and 0.0 are given in appendices 5.4 and 5.3 respectively).

First, the capacitance of the empty holder, C_H , is measured as a function of electrode separation, t_H . For two-terminal measurements using the General Radio 716-C bridge or the Boonton Q -meter, the capacitance C_H includes all capacitance beyond the coaxial switch. In this case, C_H consists of the sum of C_L (fixed lead capacitance), C_a (direct capacitance between the electrodes, $\epsilon_0 \epsilon'_N A_H / t_H$),²² and C_e (inter-electrode "edge" capacitance). For three-terminal measurements using the low-frequency apparatus C_H is the sum of C_a and C_e only.

If C_p represents the equivalent parallel capacitance of the specimen then the dielectric constant ϵ' of the material can be computed from the ratio C_p / C_v where C_v is the vacuum capacitance of the specimen, $\epsilon_0 A / t$ (see eq (3)). Assuming C_L and C_e to be unchanged by the presence of the specimen, the capacitance measured with the specimen in the holder, C_x , may be expressed as the sum of $C_p + C_H - C_A$, where C_A is $\epsilon_0 \epsilon'_N A / t_H$, the capacitance across that area, A , of the electrodes now occupied by the specimen, but previously occupied by dry nitrogen. (With the electrodes of the holder in contact with the specimen, the electrode separation t_H will in general be slightly larger than the specimen thickness t .) The expression for ϵ' may be written:

$$\epsilon' = \frac{C_p}{C_v} = \frac{C_x - C_H + C_A}{C_v} = \frac{C_x - C_H}{C_v} + \frac{t \epsilon'_N}{t_H} \approx \frac{C_x - C_H}{C_v} + \frac{t}{t_H} \quad (A-1)$$

The ratio t/t_H is always slightly less than unity. For specimens about 0.2 cm thick, t/t_H may be about 0.99. This departure from unity is due to slight surface irregularities resulting from warping or unevenness, and the thickness of the conductive coating applied to the specimen.

Equation (A-1) is applicable to measurements made at all temperatures provided the variation of C_H (at constant t_H) with temperature is known. It has been determined that C_H varies with temperature in such a way that the variation can be ascribed to the calculable change in electrode area.

The loss index is determined for the measured parallel resistance, R_p , of the specimen from the equation

$$\epsilon'' = \frac{1}{\omega R_p C_v} \quad (A-2)$$

²² A flow of dry nitrogen gas is maintained in the specimen holder so that the relative dielectric constant of nitrogen, ϵ'_N , appears in the expression for C_a .

²³ The error introduced in eq (A-1) by setting ϵ'_N equal to unity is only 0.02% for the specimens considered, for which $\epsilon' \approx 2.5$ and $t/t_H \approx 1$. We shall therefore set ϵ'_N equal to unity in the following discussions.

e. Accuracy of Measurements of ϵ' for PCTFE Disk Specimens 0.80, 0.44, and 0.73

The following discussion is given in order to determine how accurately ϵ' may be measured using the micrometer holder and techniques described above. (From eq (A-2) we see that the accuracy of ϵ'' will be determined primarily by the accuracy with which R_p can be measured. This depends primarily upon the measuring instrument. The ability of the measuring instruments to measure R_p is discussed in appendix 6, and estimates of the accuracy of ϵ'' given there.)

The accuracy with which ϵ' may be determined depends upon a number of factors, as can be seen from eq (A-1). We shall now rewrite eq (A-1) in terms of the independent variables involved and compute $\delta\epsilon'$, the error in ϵ' , from the equation

$$\delta\epsilon' = \sum \left| \frac{\partial\epsilon'}{\partial x_i} \delta x_i \right| \quad (A-3)$$

where the x_i are the independent variables and δx_i is the uncertainty in x_i .

Note that the accuracy of C_H (the capacitance of the empty holder at separation t_H) depends upon two factors—the accuracy with which the measuring device can measure capacitance, and the ability to reproducibly set the separation of the electrodes to t_H with the specimen removed. These two effects may be approximately separated by writing C_H as

$$C_H = \frac{\epsilon_0 A_H}{t_H} + (C_L + C_e) \quad (A-4)$$

Any error in t_H will be reflected in the term $\epsilon_0 A_H / t_H$ where A_H is the area of the holder's electrodes, while the error of the capacitance measuring device may be thought of as affecting the term $(C_L + C_e)$, which is essentially independent of t_H .

Equation (A-1) may now be rewritten in the form:

$$\epsilon' = \frac{(C_x - C_L - C_e)V}{\epsilon_0 A^2} - \frac{A_H V}{t_H A^2} + \frac{V}{A t_H} \quad (A-5)$$

The independently measured variables are, V , the volume of the specimen; A , the area of the specimen; t_H , and $(C_x - C_L - C_e)$.

Since

$$\frac{\partial\epsilon'}{\partial V} = \frac{\epsilon'}{V}, \quad (A-6)$$

$$\frac{\partial\epsilon'}{\partial A} = \frac{1}{A} \left[\frac{V}{t_H A} - 2\epsilon' \right],$$

$$\frac{\partial\epsilon'}{\partial(C_x - C_L - C_e)} = \frac{1}{C_v}$$

and

$$\frac{\partial\epsilon'}{\partial t_H} = \left(\frac{A_H}{A} - 1 \right) \frac{t}{t_H^2},$$

eq (A-3) becomes:

$$\delta\epsilon' = \epsilon' \frac{\delta V}{V} + \left(2\epsilon' - \frac{t}{t_H}\right) \frac{2\delta d}{d} + \frac{\delta(C_x - C_L - C_e)}{C_v} + \left(\frac{A_H}{A} - 1\right) \frac{t}{t_H} \frac{\delta t_H}{t_H}, \quad (\text{A-7})$$

where d is the diameter of the specimen.

Since V was determined by the buoyancy technique, it is given by

$$V = \frac{W_{(\text{air})} - W_{(\text{water})}}{\rho_{(\text{water})}}$$

We may write

$$\frac{\delta V}{V} = \frac{\delta W_{(\text{air})} + \delta W_{(\text{water})}}{V \rho_{(\text{water})}} + \frac{\delta \rho_{(\text{water})}}{\rho_{(\text{water})}}. \quad (\text{A-8})$$

The balance employed is accurate to 0.0001 g, and the density of water may easily be obtained to an accuracy of 0.00002 g/cm³, therefore $\delta W_{(\text{air})} = \delta W_{(\text{water})} = 0.0001$ g and $\delta \rho_{(\text{water})} = 0.00002$ g/cm³. Since $\rho_{(\text{water})} \cong 1$ g/cm³ we have,

$$\frac{\delta V}{V} = \frac{0.0002 \text{ cm}^3}{V} + 0.00002.$$

Although d could be measured to 0.0001 cm by the traveling microscope employed, in general the specimens were not perfectly cylindrical. The diameter of specimens 0.80, 0.44, and 0.73 varied from point to point by as much as 0.001 cm from their respective average values. Accordingly, δd is 0.001 cm.

t_H can be measured using a micrometer to an accuracy of at least 0.0002 cm, so that δt_H is 0.0002 cm.

We can now evaluate the accuracy of measurements of ϵ' performed on the specimens whose dimensions are given in table 1. Specimens 0.80A and 0.44A are quite similar in physical dimensions so that rough average values may be assigned for the quantities necessary to compute $\delta\epsilon'$ from eq (A-7) for these two specimens. The assigned values are: $\epsilon' = 3$, $t = t_H = 0.2$ cm, $A = 14.5$ cm², $C_v = 6.3$ pf, $d = 4.3$ cm, $V = 2.9$ cm³, and for our 2-in.-diam electrodes $A_H = 20$ cm². Using these values, eq (A-7) gives

$$\delta\epsilon' = 0.00291 + \frac{\delta(C_x - C_L - C_e)}{C_v}. \quad (\text{A-9})$$

The term $\delta(C_x - C_L - C_e)$ depends upon the accuracy of the capacitance measurement. In the case of the low-frequency bridge and the Schering bridge (described later) this is about (0.05% + 0.002pf). $\delta\epsilon'$ then becomes

$$\delta\epsilon' = 0.00291 + \frac{0.011 + 0.002}{6.3} = 0.0050.$$

This uncertainty in the value of ϵ' (0.16 percent) is the maximum error of ϵ' . The probable error is of course smaller, since some of the factors may tend to cancel one other.

If the Q -meter is employed, the error in the capacitance measurement may be as high as 0.08 pf. For specimens 0.80A and 0.44A this gives

$$\delta\epsilon' = 0.00291 + 0.0127 \cong 0.016,$$

corresponding to a maximum error of 0.5 percent in ϵ' . The Q -meter is of course less accurate than the bridges employed at lower frequencies.

The error involved in measurements of ϵ' on specimens 0.80B, 0.44B, and 0.73 may be similarly calculated. These specimens have quite similar physical dimensions. Assuming that $\epsilon' = 3$, $t = t_H = 0.2$ cm, $A = 5$ cm², $C_v = 2.2$ pf, $d = 2.5$ cm, $V = 1$ cm³, and $A_H = 20$ cm², we have from eq (A-7),

$$\delta\epsilon' = 0.00766 + \frac{\delta(C_x - C_L - C_e)}{C_v}. \quad (\text{A-10})$$

If the low-frequency bridge or Schering bridge is employed we have:

$$\delta\epsilon' = 0.00766 + \frac{0.0066 + 0.002}{2.2} = 0.0116.$$

If the Q -meter is used,

$$\delta\epsilon' = 0.044.$$

From the above considerations it is apparent that the data obtained from specimens 0.80A and 0.44A are more accurate than the data from specimens 0.80B, 0.44B, and 0.73. In this regard we shall now indicate the frequency range over which dielectric measurements were made upon the various individual specimens. Measurements on specimens 0.80A and 0.44A were made using the Schering bridge and the Q -meter covering the frequency interval from 50 c/s to 10 Mc/s. These specimens were then cut down in diameter to form 0.80B and 0.44B, which were measured using the re-entrant cavity and the low-frequency bridge (0.01 to 200 c/s). The values of ϵ' obtained using the low-frequency bridge on these specimens have a possible error of about 0.4 percent, as compared to an error of 0.16 percent in the data taken on specimens 0.80A and 0.44A with the Schering bridge. Occasional discrepancies between the two sets of ϵ' data were then remedied by shifting the low-frequency data by a constant amount to match that from the Schering bridge in the region of overlap (50 to 200 c/s). Since both sets of data are internally consistent to much better than 0.1 percent, then the error in the resulting ϵ' values for specimens 0.80 and specimens 0.44 is about 0.16 percent in the frequency interval from 0.1 c/s to 100 kc/s. From 100 kc/s to 10 Mc/s the uncertainty may be as high as 0.5 percent.²⁴

²⁴ A detailed comparison of the ϵ' values obtained by the two-terminal method for disk specimens described here, and three-terminal measurements on specimens of similar size, has been made in our laboratory on a number of materials with moderate to low dielectric constants. Several of these had properties resembling PCTFE. These results, carried out from 100 c/s to 100 kc/s, clearly show that the two- and three-terminal methods give ϵ' values that generally agree to within 2 parts in 1,000, the error being random. It is clear from this and similar studies at lower frequencies [5] that the results on the disk specimens of PCTFE are free from fringing effects.

At all temperatures the ϵ' data obtained on specimens 0.80A and 0.80B under the same experimental conditions agreed to within 0.01. The data taken on specimens 0.44A and 0.44B, while showing equally good agreement at temperatures below 50 °C, deviated by as much as 0.027, or about 1 percent at 118 °C. It is possible that these more amorphous specimens may have become distorted at these elevated temperatures due to the slight compressive force of the electrodes. In any event, average values are given in this temperature region so that the error may be as high as about 0.5 percent.

The accuracy of measurements of ϵ' for specimen 0.73 has been previously discussed. In this case occasional mismatches in ϵ' values obtained on the low-frequency bridge and on the Schering bridge were remedied by shifting both sets of data to their average value in the region of overlapping frequency. The maximum shift in ϵ' required to match the data at any temperature was 0.004 or about 0.1 percent. The maximum uncertainty was previously calculated as about 0.4 percent in the frequency interval from 0.1 c/s to 100 kc/s and about 1.5 percent from 100 kc/s to 10 Mc/s.

Measurements of the liquid specimen are discussed in appendix 5.3, while a detailed consideration of the accuracy of thin film measurements is given in appendix 5.4.

5.3. Measurements on Pure Liquid (Specimen 0.0). Three-Terminal Modification of Micrometer Holder

Above its melting temperature (224 ± 1 °C, [7]) PCTFE is a very viscous liquid. Although gross deformation of the specimen did not take place in dielectric measurements up to 250 °C, there was sufficient change of the specimen's area due to deformation to cause some doubt as to the accuracy of the results obtained using the technique of measurement outlined in appendix 5.2. To remove this uncertainty in the area, the specimen holder was equipped with a guard ring. With this arrangement three-terminal measurements were made upon a specimen of PCTFE (specimen 0.0) whose diameter was greater than that of the inside diameter of the guard ring. Changes in the specimen's area became unimportant since the area involved in computing C_v was then the equivalent area of the guarded electrode [38].

a. Holder Modifications, Guard Ring

The following is a brief description of the modification of the specimen holder, previously discussed in section 5.1b.

A stainless steel guard ring was attached to the movable electrode by four 0.125-in.-diam sapphire rods which pass horizontally through the guard ring and into the guarded electrode at 90° intervals. The sapphire rods were fitted tightly into carefully machined holes and held the guard ring in place with good rigidity.

The gap width between the guarded and guard electrodes was 0.0499 cm. The guard ring was grounded through a silver wire.

The diameter of the fixed unguarded electrode was increased to match the outside diameter of the guard ring (6.46 cm) by attaching a stainless steel circular plate to the smaller fixed electrode. This plate was machined so that a large shoulder extends down over the edge of the smaller electrode, serving to center the plate accurately on the smaller electrode. The plate and smaller electrode are tightly held together by three screws which pass horizontally through tapped holes in the shoulder and bear against a groove on the side of the smaller electrode.

All metal parts are made of stainless steel and have been gold plated.

In order to increase the electrical resistance between the movable guarded electrode and the ceramic plate which supports it, fused silica washers and spacers have been installed between all areas of contact.

This guarded electrode arrangement has been used only up to 250 °C. There is no apparent reason, however, why it could not be employed up to 500 °C.

b. Experimental Procedures

The specimen employed (specimen 0.0) was a disk about 5.4 cm in diameter and 0.2 cm thick. No surface electrodes were applied, since after heating to 250 °C the specimen and electrodes made good adhesive contact.

The dielectric measurements were first made near 250 °C, then near 220 °C, then near 200 °C. Measurements at 200 °C, where the specimen is in the supercooled liquid state, must be made as rapidly as possible since crystallization will become noticeable after about an hour [7]. Furthermore, since degradation takes place after prolonged exposure to temperatures above the melting point, these measurements were performed as rapidly as possible and in a nitrogen atmosphere.

The imminence of crystallization at one thermal extreme and the possibility of degradation at the other, made it unwise to take the time to cover more than a limited portion of the frequency spectrum. Three-terminal measurements were made only between 20 and 200 c/s.

Knowing the capacitance, C_H , as a function of the electrode separation, t_H , from experiment, the dielectric constant can be computed from the measured capacitance, C_x , by the equation

$$\epsilon' = \frac{C_x}{C_H} \quad (\text{A-11})$$

c. Accuracy

The error involved in the determination of ϵ' is given by

$$\delta\epsilon' = \frac{\epsilon'}{C_x} \delta C_x + \frac{\epsilon'}{C_H} \delta C_H \quad (\text{A-12})$$

The quantity δC_H consists of two parts: (a) the bridge uncertainty $\pm (0.05\% + 0.002 \text{ pf})$ and (b) the error due to our uncertainty in the value of t_H

(0.0002 cm). Therefore

$$\delta C_H = 0.002 \text{ pf} + 0.0005 C_H + C_H \frac{\delta t_H}{t_H} \quad (\text{A-13})$$

Since $C_H = 8.4 \text{ pf}$ and $t_H = 0.22 \text{ cm}$ this becomes

$$\delta C_H = (0.002 + 0.004 + 0.0076) \text{ pf} = 0.0136 \text{ pf} \quad (\text{A-14})$$

Substituting this into eq (A-12), with $C_x \approx 22 \text{ pf}$, and $\delta C_x = \pm (0.05\% + 0.002 \text{ pf})$ gives

$$\frac{\delta \epsilon'}{\epsilon'} = 0.0006 + 0.0016 = 0.0022. \quad (\text{A-15})$$

Therefore the calculated percentage error is 0.22 percent.

This apparent accuracy will be achieved however, only under ideal conditions, in particular only if the specimen and the electrodes make perfect contact. Inspection of the surface of the specimen after removal from the holder²⁵ showed no signs of bubbles or irregularities, indicating that the contact with the electrodes was good. To be safe, however, the uncertainty in the values of ϵ' given in table 6 is stated as ± 0.5 percent.

5.4. Thin Film Measurements (Specimen 0.12)

It is difficult to determine the dielectric properties of thin films with high accuracy. The most accurate results appear to be obtained by using the liquid displacement technique. This involves computing the dielectric properties of the specimen from the change in capacitance and resistance which results when the film is placed between the plates of a test cell containing a nonsolvent liquid whose dielectric properties are known. A complete description of this method is given elsewhere [39]. For the present application such a procedure was not adopted since it would have substantially prolonged the experimental phase of this investigation. The measurements of thin films reported here were made using the specimen holder with the guard ring attached as described in sec. 5.2. Three-terminal measurements were made up to 200 c/s using the low-frequency bridge modified to measure higher values of capacitance and conductance. Two-terminal measurements were made between 50 c/s and 200 kc/s after shorting the guarded electrode to ground.

The specimen was cut from a quenched thin film to have a diameter greater than that of the holder's guarded electrode. A guarded specimen electrode (slightly smaller than that of the holder's), a guard ring, and an unguarded electrode were applied to the specimen with silver conducting paint. Evaporated gold was not used because it was feared that the specimen might be excessively heated at its surface and thus crystallize locally. (The series resistance

of the conducting paint led to no perceptible anomalous behavior in the measured loss up to 200 kc/s.) The specimen's average thickness, $t = 0.01464 \text{ cm}$, was determined using the buoyancy technique (sec. 2.3) before applying the surface electrodes.

a. Three-Terminal Measurements on Films

The basic equation used to compute the dielectric constant from the three-terminal measurements is:

$$\epsilon'_m = C_x / C_v, \quad (\text{A-16})$$

where C_x is the measured three-terminal capacitance of the holder with the specimen between the electrodes and C_v is the vacuum capacitance computed using the specimen's average thickness and the area of the holder's electrodes. This equation, however, neglects several factors which require closer inspection when thin films are considered.

Surface Irregularities. Surface irregularities or roughness may become an important consideration where thin films are concerned since there it leads to a proportionally greater percentage variation in the thickness of the specimen. The effect of such irregularities is treated below in an approximate manner.

Let the plane surface area of a disk-shaped specimen be divided by a grid coordinate system into n small areas, each with area ΔA . Assuming that the field in the dielectric is everywhere perpendicular to the plane of the faces, then the total parallel capacitance of the system, C_{pm} , becomes:

$$C_{pm} = \epsilon' \epsilon_0 \Delta A \sum_{i=1}^n \frac{1}{t_i} \quad (\text{A-17})$$

Here t_i is the separation between the faces at the i th segment of area.

The average thickness, t , determined by the buoyancy method is

$$t = \frac{1}{n} \sum_{i=1}^n t_i. \quad (\text{A-18})$$

Since t_i may be written as

$$t_i = t + (t_i - t) = t \left[1 + \frac{t_i - t}{t} \right], \quad (\text{A-19})$$

then if $1/t_i$ is expanded in a binomial series, C_{pm} becomes:

$$C_{pm} = \frac{\epsilon' \epsilon_0 n \Delta A}{t} \left(1 + \frac{1}{n} \sum_i \left[\left(\frac{t_i - t}{t} \right)^2 - \left(\frac{t_i - t}{t} \right)^3 + \dots \right] \right) \quad (\text{A-20})$$

Dropping cubed and higher order terms and letting $n \Delta A = A$ we have²⁶

$$C_{pm} = C_p \left[1 + \left(\frac{\sigma}{t} \right)^2 \right]. \quad (\text{A-21})$$

²⁵ It was necessary to dip the electrode assembly into liquid N_2 in order to remove the specimen from between the electrodes. This severe thermal shock did no apparent damage to either the specimen or the electrodes. The sapphire rods holding the guard ring in place were removed prior to this thermal shock.

²⁶ Calculation of the effects of surface irregularities with eq (A-21) will lead to a lower limit to the actual capacitance. It will be sufficiently accurate provided the surface is reasonably smooth, possessing very few sharp discontinuities, and also provided the undulations of the surface have "wavelengths" considerably greater than the specimen's thickness.

Here C_p is the parallel capacitance of the specimen calculated using the average thickness and σ is the standard deviation from the average thickness defined as:

$$\sigma = \left[\frac{\sum_{i=1}^n (t_i - t)^2}{n} \right]^{1/2} \quad (\text{A-22})$$

Dividing eq (A-21) by C_v gives

$$\epsilon'_m = \epsilon' \left[1 + \left(\frac{\sigma}{t} \right)^2 \right], \quad (\text{A-23})$$

where ϵ'_m is the apparent or measured dielectric constant and ϵ' is the true value. This result shows that surface irregularities will always give rise to an apparent increase in the dielectric constant. The extent of the increase is governed by the square of the ratio (σ/t) and will therefore be more significant the thinner the specimen.

A convenient method of roughly evaluating σ is through micrometer measurements. Assuming that N micrometer readings are taken over the surface of the specimen, then the standard deviation, σ_r , of these readings, t_m , from the true mean, t , is

$$\sigma_r = \left[\frac{\sum_{m=1}^N (t_m - t)^2}{N} \right]^{1/2} \quad (\text{A-24})$$

Since in most cases, σ_r will be slightly greater than σ , use of σ_r in place of σ will set an upper limit for the effect of surface irregularities. This method is equally applicable to specimens whose surfaces are slightly tilted.

For specimen 0.12, on the basis of some forty micrometer readings, σ_r was found to be 0.00107 cm, so that $(\sigma_r/t)^2$ is 0.0053. Therefore, to correct for the effect of surface irregularities, the measured value of ϵ' was reduced by about 0.5 percent.

Effects of specimen electrodes. It is obvious that for very thin specimens the thickness of the guarded surface electrode painted on the specimen may become important. If this electrode is sufficiently thick, a slight fringing field will be set up at its edge, tending to increase the capacitance.

Since the surface electrodes were about 0.0048 cm thick, and the specimen's thickness was only 0.01464 cm, a calculation of the possible magnitude of this effect was made.

Adopting an equation of W. R. Smythe [40] to describe the situation at hand, it was found that the capacitance increase due to the edge of the painted electrode was only about 0.07 percent of the total capacitance.

A far more important effect than this is produced by the fact that the area of the painted guarded electrode was smaller by about 7.4 percent than the area of the guarded electrode of the specimen holder. This leaves an air gap between the specimen and the holder's electrode in the uncoated region. The effect of this air gap is to reduce the measured capacitance, or equivalently, to lower the calculated value of ϵ' .

A calculation showed that the measured value of ϵ' should be increased on the average 3.5 percent to compensate for this uncoated area. This correction is slightly dependent on ϵ' and this dependence was included in the calculated correction.

Summary. Surface irregularities can be corrected for by reducing ϵ'_m by 0.5 percent. The effects of the air film near the edge of the guarded electrode may be corrected for by increasing ϵ'_m by 3.5 percent. The small fringing capacitance from the edge of the painted guarded electrode may be compensated for by decreasing ϵ'_m by about 0.1 percent. Therefore, summing these, the true value of ϵ' is attained by increasing ϵ'_m by about 2.9 percent. The values of dielectric constant for specimen 0.12 reported in table 5 include these corrections. The accuracy of the reported values of ϵ' is estimated to be about ± 1 percent.

b. Two-Terminal Measurements of Films

As indicated earlier, two-terminal measurements on specimen 0.12 were made up to 200 kc/s by shorting the guarded electrode to ground. Corrections were applied to the two-terminal measurements to compensate for the same factors which influenced the three-terminal measurements discussed above. The corrections to ϵ' (about 7%) were larger, however, due to the air film near the specimen's edge. After correction, the two-terminal and three-terminal measurements in the region of overlapping frequencies agreed to within 1 percent. The two-terminal data, which contained larger corrections, were then shifted to match the presumably more accurate three-terminal data.

c. Corrections to ϵ''

By methods similar to those discussed in section 5.4a, the effects of the factors mentioned upon measurements of ϵ'' were calculated and corrected. The net correction to the three-terminal measurements of ϵ'' was about a 4.5 percent increase. Two-terminal measurements required corrections near 14 percent. The accuracy of the values in ϵ'' given in table 5 is about ± 3 percent.

6. Appendix. Impedance-Measuring Devices Covering 0.01 c/s to 10 Mc/s for Use with Micrometer Specimen Holder

Three different instruments were employed to measure the dielectric properties of the PCTFE specimens over the broad frequency range from 0.1 to 10^7 c/s with the micrometer specimen holder. The following sections give discussions of each of these instruments, including their accuracy. Estimates of the accuracy of the ϵ'' measurements are given special emphasis.

6.1. Ultra-Low-Frequency Bridge

The low-frequency bridge operates in the frequency range of 0.01 to 200 c/s. It measures parallel capacitances between 0 and 100 pf, and conductances between 10^{-9} and 10^{-15} mhos. Under suitable conditions accuracies of $\pm(0.05$ percent

+ 0.002 pf) in capacitance and about $\pm(1 \text{ percent} + 3f \times 10^{-15} \text{ mhos})$ in conductance are achieved. (Here f is the frequency in c/s.) The dielectric constant, ϵ' , of a material can therefore be determined to an accuracy proportional to that of the capacitance measurements. The loss index is measured to an accuracy of about $\pm(1\% + 5 \times 10^{-4}/C_v)$ where C_v is the equivalent vacuum capacitance expressed in pf.

The low-frequency bridge employed is similar to the bridge of Weingarten [41] which is described also by Heroux [42]. It is a three-terminal device, but it is unnecessary to balance a separate guard circuit. A complete description and demonstration of the capabilities of the low-frequency apparatus employed here is given elsewhere [5].

6.2. Schering Bridge

A modified General Radio type 716-C Schering bridge is employed in the frequency range of 50 c/s to 200 kc/s. The bridge was modified as follows. The 100- to 1100-pf variable capacitor was removed from the bridge and replaced by a dual range (25 to 110 pf and 250 to 1100 pf) variable capacitor. This modification allows greater accuracy in the measurement of both low capacitances and low conductances. The capacitor is equipped with an additional reduction gear and scale which allows one to measure capacitances to a precision of 0.001 pf on the low range.

The substitution method is employed. Capacitances may be measured on the low range to an accuracy of about $\pm(0.05 \text{ percent} + 0.002 \text{ pf})$ once the measuring capacitor is calibrated. The loss index ϵ'' may be measured to an accuracy of about $\pm(2 \text{ percent} + 1 \times 10^{-3}/C_v)$ where C_v is in pf.

In order to realize the full capability of this apparatus in the measurement of capacitance it is necessary to use rigid coaxial leads to connect the bridge and specimen holder. This minimizes the small erratic capacitance changes due to small physical motions which may occur if flexible coaxial leads are employed.

Adequate sensitivity is provided by a tunable null indicator (Rhode and Schwarz Type UBM) with only 15 v applied to the bridge by the signal generator (Hewlett Packard, Model 200-C).

6.3. Q-Meter

In the frequency range of 100 kc/s to 10 Mc/s a Boonton Radio Corporation type 160-A Q-meter is employed. This instrument has been modified and is now equipped with a " ΔQ -meter" to facilitate more sensitive measurements on low values of parallel conductances. The ΔQ -meter also allows one to tune more accurately to the resonance peak.

Since we attempted to achieve accuracies greater than those which the instrument was designed to deliver, special mention of the calibration procedure employed is given here.

a. Calibration and Operation

First the parallel variable resonating capacitors are calibrated as follows. (All operations are best

carried out with the Q-meter turned on and in warmed up condition.) The main capacitor is carefully set²⁷ on its lowest indicated value (30 pf). With the vernier capacitor carefully set to zero, the capacitance terminals are connected to the Schering bridge which is then balanced at a frequency near 1 kc/s. The frequency 1 kc/s is chosen so as to avoid inductive effects in the leads connecting the Q-meter and bridge. Now the setting of the main capacitor of the Q-meter is increased, carefully setting 5 pf higher on the scale. The change in actual capacitance required to rebalance the Schering bridge gives the capacitance change between these two settings. This procedure is then repeated at each 5-pf interval along the scale until the required range is covered. Thus a relative calibration of the main capacitor is achieved. The vernier capacitor (scale reads -3 to +3 pf) is similarly calibrated at each 0.1-pf setting.

With the resonating capacitors now calibrated at 1 kc/s we make the assumption that this calibration remains constant with frequency up to 10 Mc/s. The problem of series inductance and resistance in the leads to the sample holder will be discussed later. Before doing so however, let us first outline the operational procedure followed in measurements of unknown impedances.

The micrometer specimen holder (previously described) containing the specimen is connected to the Q-meter through rigid coaxial leads which should be as short as possible. With the switch I of figure 26 open, the Q-meter is roughly resonated at the selected frequency by suitable choice of the coil and by varying the main capacitance setting. Next the main capacitor is set to the nearest 5-pf calibration point and resonance achieved by adjusting the vernier. The Q reading is then recorded (Q_1) as well as the readings of the capacitors which when corrected and summed give a capacitance C_1 . Now the switch I is closed. Resonance is restored by decreasing C. At resonance, with the unknown in, the Q reading (Q_2) is recorded as well as the corrected capacitance reading, C_2 . The measured parallel capacitance to ground beyond the switch is simply $C_M = C_1 - C_2$ from which the dielectric constant of the unknown may be determined from eq (A-1) by setting $C_x = C_M$ (if lead inductance is neglected). The loss index of the unknown is given by

$$\epsilon'' = \frac{C_T}{C_v} \left(\frac{1}{Q_2} - \frac{1}{Q_1} \right), \quad (\text{A-25})$$

where C_T is the total capacitance required to resonate the coil at the operating frequency. (C_T may be determined separately.)

b. Accuracy

The accuracy with which capacitance can be measured is limited essentially by the accuracy with

²⁷ The Q-meter has been equipped with a device to eliminate the effect of parallax from the reading of the main capacitor. This device consists of a one inch length of $\frac{1}{2}$ -in.-o.d. polymethylmethacrylate (PMMA) rod which has been split and one-half mounted over the fiducial line of the capacitor. A fine line has been inscribed on the outer rounded surface of the PMMA section parallel to the fiducial line. With this device the capacitor can be set at calibrated values up to 100 pf to within ± 0.01 pf.

which the main capacitor can be set to the calibrated 5-pf intervals. With care this setting is reproducible to ± 0.01 pf up to about 100 pf. Since the substitution method is employed the capacitance can be measured to an accuracy of about ± 0.02 pf.

One may compute the error in ϵ'' ($\delta\epsilon''$) using the general method of eq (A-3). Equation (A-25) in terms of independent variables becomes

$$\epsilon'' = \frac{C_T}{C_v} \left(\frac{\Delta Q}{Q_1 Q_2} \right), \quad (\text{A-26})$$

Here ΔQ , $(Q_1 - Q_2)$, is an independent variable since it is independently measured using the ΔQ -meter attachment. Neglecting the comparatively small uncertainty in C_v the following relationship is derived

$$\frac{\delta\epsilon''}{\epsilon''} = \frac{\delta Q_1}{Q_1} + \frac{\delta Q_2}{Q_2} + \frac{\delta C_T}{C_T} + \frac{\delta \Delta Q}{\Delta Q}. \quad (\text{A-27})$$

The term $\delta C_T/C_T$ is in general about 1pf/100 pf. The remaining three terms all consist of two parts. One part is the calibration error of the appropriate voltmeter (either the Q - or ΔQ -voltmeter) which, in both cases, we assume is one percent. The other part is the resolution with which the voltmeters can be read. The Q voltmeter can be read to about ± 1 (full scale 250). The limit of resolution on the ΔQ -voltmeter is about ± 0.2 (full scale 50). Assuming that $Q_1 \cong Q_2 \cong 200$,

$$\frac{\delta\epsilon''}{\epsilon''} = 0.05 + \frac{0.2}{\Delta Q}. \quad (\text{A-28})$$

Eliminating ΔQ by use of eq (A-26) and substituting the above approximate numerical values gives

$$\delta\epsilon'' = \pm \left(5\% + \frac{5 \times 10^{-4}}{C_v} \right), \quad (\text{A-29})$$

where C_v is in picofarads.

c. Lead Corrections

Certain corrections due to series inductance and resistance become important at high frequencies.

A lead inductance L in series with the holder capacitance C_x gives rise to an apparent capacitance C_M which is given by the equation

$$C_M = \frac{C_x}{1 - \omega^2 L C_x},$$

or

$$C_{Mx} \equiv C_M - C_x = \omega^2 L C_x C_M = \omega^2 L C_M^2 / (1 + \omega^2 L C_M). \quad (\text{A-30})$$

Furthermore, a resistance R_s in series with the equivalent capacitance C_M gives rise to a loss tangent for the empty holder given by the expression

$$(\tan \delta)_e = \omega R_s C_M = \frac{C_T}{C_M} \left(\frac{1}{Q_2} - \frac{1}{Q_1} \right). \quad (\text{A-31})$$

Defining $\Delta(1/Q)_e$ as the $(1/Q_2 - 1/Q_1)$ observed when the holder contains no sample, eq (A-31) may be rewritten as

$$\Delta \left(\frac{1}{Q} \right)_e = \frac{\omega R_s C_M^2}{C_T}. \quad (\text{A-32})$$

Thus for a particular coil ($C_T = \text{constant}$), at a particular frequency, eqs (A-30) and (A-32) show that $(C_M - C_x)$ and $\Delta(1/Q)$ are functions of C_M and that experimentally derived plots of $(C_M - C_x)$ and $\Delta(1/Q)_e$ versus C_M can be used to correct for the effects of L and R_s . For convenience $(C_M - C_x)$ is defined as C_{Mx} .

Graphs of C_{Mx} and $\Delta(1/Q)_e$ were obtained in the following manner. The capacitance C_x of the empty holder at a particular electrode separation was determined at 1 kc/s using the Schering bridge. The holder was then connected to the Q -meter and C_M and $\Delta(1/Q)_e$ determined at the desired frequencies. This procedure was then repeated at different electrode separations so that values of C_x covering the desired range were measured. Completion of the experiment outlined above yielded data from which C_{Mx} and $\Delta(1/Q)_e$ versus C_M curves were drawn.

The dielectric properties of a specimen were determined as follows. With the specimen in the holder C_M and $\Delta(1/Q)_M$ were determined. C_M is the change in capacitance required to reresonate the system after switching the holder out. $\Delta(1/Q)_M$ is the measured change in $1/Q$. From the appropriate calibration curve the value of C_{Mx} at the observed C_M was obtained. C_x was obtained from the equation

$$C_x = C_M - C_{Mx}. \quad (\text{A-33})$$

The dielectric constant of the specimen is then given by eq (A-1).

The value of $\Delta(1/Q)_e$ at the observed value of C_M was obtained from the calibration curve. If R_{sx} is the series resistance of the specimen then the measured $\tan \delta$ is given by the approximate relation,

$$\tan \delta_M = \omega C_M \left(R_s + R_{sx} \frac{C_p^2}{C_x^2} \right) = \frac{C_T}{C_M} \Delta \left(\frac{1}{Q} \right)_M. \quad (\text{A-34})$$

where C_p is the parallel capacitance of the specimen. From eqs (A-31) and (A-34) it is easy to show that

$$\epsilon'' = \left(\frac{C_x}{C_M} \right)^2 \frac{C_T}{C_v} \left[\Delta \left(\frac{1}{Q} \right)_M - \Delta \left(\frac{1}{Q} \right)_e \right]. \quad (\text{A-35})$$

In all the above equations it is assumed that $\tan \delta$ of the specimen is sufficiently small so that the equivalent parallel and series capacitance of the specimen are nearly the same. Values of $\tan \delta$ up to 0.1 fulfill this restriction reasonably well.

At frequencies above about 3 Mc/s these corrections become significant. The accuracy of the measurements is reduced in some cases because the magnitude of the correction approaches the specimen's contribution to the measured quantity. Measurements of capacitance may err by ± 0.08 pf. The accuracy of loss index measurements becomes roughly $\pm (7 \text{ percent} + 0.001/C_v)$ where C_v is in pf.

7. Appendix. High-Frequency Measurements (290 Mc/s to 8.6 kMc/s)

Two separate instruments were used to determine ϵ' and ϵ'' at high frequencies. These are briefly described below. The description of these devices has been separated from that of instruments employed at lower frequencies for the reason that the operating principle is quite different.

7.1. Re-entrant Cavity

Figure 27 shows a cross section of the re-entrant cavity used for the measurements at 290 Mc/s. It is similar in most respects to re-entrant cavities

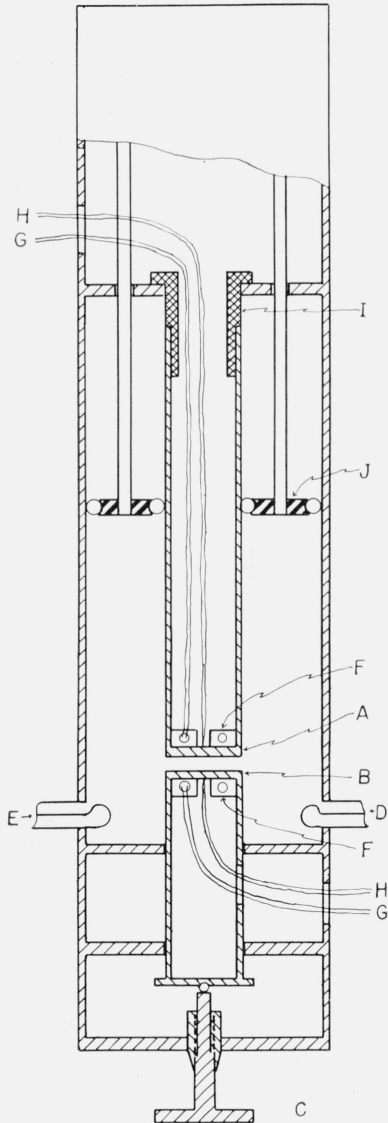


FIGURE 27. The re-entrant cavity.

- | | |
|-----------------------|------------------------|
| A = Fixed electrode | F = Heater elements |
| B = Movable electrode | G = Heater wires |
| C = Micrometer screw | H = Thermocouple wires |
| D = Input loop | I = Ceramic insulator |
| E = Detector loop | J = Movable short |

described previously by Parry [43], Works [44], and Reynolds [45]. One feature which distinguishes this instrument is the variable length of the cavity effected by means of a sliding short (**J** in the diagram). This feature allows more flexibility in the selection of sample size and resonant frequency than is possible in a cavity of fixed length. It also simplifies the capacitance calibration: The short is withdrawn to the uppermost end of the cavity where it is insulated from the upper conductor by a ceramic insulator **I**. In this configuration it is possible to measure the interelectrode capacitance as a function of the micrometer setting using a Schering bridge at 1 kc/s.

Measurements at temperatures above room temperature were achieved by means of heaters inside the ends of the electrodes. The end pieces could be maintained at temperatures up to 150 °C by separate control of the electrode heaters, **G**, using thermocouples, **H**, in each electrode. The interelectrode capacitance became somewhat uncertain at temperatures much above 150 °C due to thermal fluctuations along the supporting cylinders.

A block diagram of the cavity and the associated equipment is shown in figure 28. A Rollin Model 30A signal generator served as a signal source. As indicated, this signal was mixed with that from a low power signal generator operating within a few megacycles of the resonance frequency and the beat frequency was measured with a Collins radio receiver. Frequency changes of the driving generator were measured in this manner to an accuracy of 1 kc/s during the dielectric loss measurements as described below. A 1 kc/s modulation was applied to the signal source to facilitate detection. A bolometer and Hewlett Packard standing wave indicator (Model 415-B) were used for detection.

The measurements of dielectric constant and loss index were carried out in much the same manner as has been described by previous authors. The disk-shaped specimen (0.80B or 0.44B) was placed between the electrodes which then maintained a slight pressure on the specimen. The sliding short

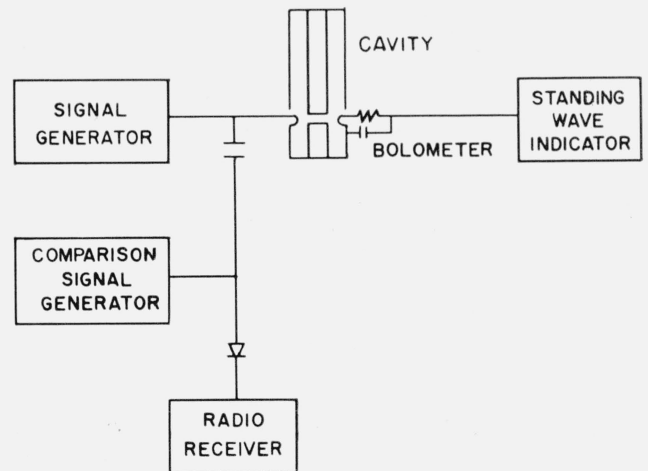


FIGURE 28. Block diagram of the re-entrant cavity and ancillary equipment.

was adjusted to achieve resonance after the generator had been set to the desired frequency. The electrode spacing was measured to an accuracy of about 1 μ . The sample was then removed and the electrode spacing readjusted to achieve resonance. From the calibration of the interelectrode capacitance it was possible to compute the capacitance of the sample and thus the dielectric constant.

Several methods have been described for measurements of the dielectric loss index. Essentially they are all one of two general types: in one case the Q of the empty cavity and the cavity with the sample in place are measured independently and thence the dissipation of the sample computed. An alternative method involves measurements of the Q of the empty cavity and the computation of the Q of the cavity with the sample from comparison of the voltage at resonance for the two conditions. The Q of a resonant cavity can be measured by obtaining the shape of the resonance curve either by small changes in the capacitance of the cavity or by small change of the frequency of the driving generator. Due to the sliding short, the cavity could not be equipped with a vernier capacitor such as Reynolds [45] used, and the capacitance could only be changed by altering the electrode spacing. The Q of the empty cavity was so high that, in general, a change of interelectrode spacing of only a few microns was sufficient to achieve the half-resonance-voltage condition. Accurate determination of the Q of the empty cavity by this method was out of the question. Obviously this method could not be used when a sample was in the cavity fixing the interelectrode spacing. The frequency shift method was therefore used. The relation for computing the loss index is

$$\epsilon'' = \frac{(dC/df)(\Delta f_2 - \Delta f_1)}{C_v \sqrt{q-1}} \quad (\text{A-36})$$

in which the differential dC/df is determined by varying the electrode separation of the empty cavity (and thus the capacitance) by a small amount and observing the change in the resonance frequency over a narrow range near the frequency of the measurement. The quantities Δf_1 , and Δf_2 are the frequency shifts from the resonant frequency for the empty and sample-loaded cavity required to observe a voltage V_r/\sqrt{q} where V_r is the peak resonant voltage.

An alternate method of measuring dielectric loss, which is particularly suitable where the loss is small, involves the measurement of the ratio, $(V_1 - V_2)/V_2$, where V_1 is the resonant voltage with the sample out and V_2 that with the sample in the cavity. The relationship for computing the loss is then

$$\epsilon'' = \frac{(dC/df)\Delta f_1(V_1 - V_2)/V_2}{C_v \sqrt{q-1}} \quad (\text{A-37})$$

It is clear that where the difference $(\Delta f_2 - \Delta f_1)$ is small, i.e., the loss is small, this technique improves the accuracy of the measurement. The detection system used in this work gave the voltage difference

in decibels, which was conveniently converted by means of the expression

$$\frac{V_1 - V_2}{V_2} = \left[\text{antilog} \left(\frac{db}{10} \right) \right] - 1. \quad (\text{A-38})$$

Where suitable, these two methods of measurement gave loss values in close agreement, rarely differing by more than 2 percent.

The dielectric constants are estimated to be accurate to about 0.5 percent, the error being chiefly due to uncertainty of the interelectrode spacing of the empty cavity. The dielectric loss indexes are estimated to be accurate within 5 percent. In this case the errors are principally due to slight deviations from square law detection and variations in output level of the signal generator, particularly with small changes in frequency. Both these sources of error could undoubtedly be reduced, but it was believed that any real improvement in performance would require an unjustifiable amount of effort.

7.2. Microwave Apparatus

The dielectric properties of PCTFE at microwave frequencies were determined at room temperature (23 °C) with a Microwave Dielectrometer (Model 2), manufactured by Central Research Laboratories, Inc.

The principle of the Dielectrometer has been extensively discussed by Roberts, von Hippel, Westphal, and others [46, 47]. The instrument has a slotted, circular waveguide which may be operated at frequencies of 1, 3, and 8.6 kMc/s. At 8.6 kMc/s the waveguide is excited in the TE_{11} mode by reflex klystrons. At 1 and 3 kMc/s a center conductor is introduced so that the waveguide becomes a coaxial line, excited by klystrons in the TEM modes. One end of the waveguide is shorted, and the standing wave is measured by a precision traveling probe, which acts as a square law detector.

The introduction of a dielectric specimen, which fills the end of the waveguide and which presents plane faces perpendicular to the waveguide axis, establishes a new standing wave pattern. The traveling probe is used to determine the distance of the node from the shorted end, X_0 , and to determine the distance between double power points, ΔX . This information, together with the length of the dielectric specimen, d , and the distance between nodes in the guide $\lambda/2$, is used to determine the propagation constant of the specimen, γ :

$$\frac{\tanh \gamma d}{\gamma d} = -\frac{\lambda}{2\pi d} \frac{\tan(2\pi X_0/\lambda) + j \frac{\sin(\pi \Delta X/\lambda)}{[1 + \sin^2(\pi \Delta X/\lambda)]^{1/2}}}{1 - j \frac{\sin(\pi \Delta X/\lambda)}{\sqrt{1 + \sin^2(\pi \Delta X/\lambda)}} \tan\left(\frac{2\pi X_0}{\lambda}\right)} \quad (\text{A-39})$$

Equation (A-39) is easily determined by transmission line theory [46]. After γ is determined we find the

dielectric properties from the equation [46]

$$\epsilon' - j\epsilon'' = \frac{(\lambda_c)^{-2} - \left(\frac{\gamma d}{2\pi d}\right)^2}{(\lambda_c)^{-2} + (\lambda)^{-2}}, \quad (\text{A-40})$$

where the cut off wavelength of the TE₁₁ mode at 8.6 kMc/s is $\lambda_c = 43.43$ mm, while the cut off wavelength of the TEM modes at 1 kMc/s and 3 kMc/s is $\lambda_c = \infty$.

Small corrections due to the attenuation of the empty waveguide must be made to eqs (A-39) and (A-40) above. These corrections are described in the literature (see, e.g., Westphal [47].)

The accuracy of the measurements require that the specimen be accurately machined so that the end of the waveguide is filled snugly, with the plane faces perpendicular to the waveguide axis. Two circular cylindrical samples were made from stock of PCTFE. This stock had a specific volume of 0.4657 cm³/g upon receipt. After a six-day heat treatment where the stock was held for extended periods at temperatures of 200, 190, 180, and 170 °C, the specific volume at 23 °C was decreased to 0.4629, which corresponds to a degree of crystallinity of 0.78 [4]. From this stock two right circular cylindrical specimens of 2.542-cm diam were machined with the plane faces accurately perpendicular to the cylindrical axis. The specimen which was used at 8.6 kMc/s had a length of 1.916 cm. The second specimen, used at 1 and 3 kMc/s, had a length of 3.179 cm, and had an accurately concentric center hole with a diameter of 0.950 cm to fit the coaxial center conductor of the instrument.

These specimens were then used for the determination of the dielectric constant and loss index at room temperature at frequencies of 1, 3, and 8.6 kMc/s. The results are included in table 2.²⁸

²⁸ Because of the large samples that are required for the microwave apparatus, it was impossible to quench them to achieve a crystallinity as low as that of specimen 0.44.

8. References

- [1] S. I. Reynolds, V. G. Thomas, A. H. Sharbaugh, and R. M. Fuoss, *J. Am. Chem. Soc.* **73**, 3714 (1951).
- [2] L. Hartshorn, J. V. L. Parry, and E. Rushton, *J. I.E.E.* **100**, Pt. 11A, No. 3 (1953).
- [3] G. P. Mikhailov and B. I. Sazhin, *Soviet Phys. Tech. Phys.* **1**, 1670 (1957). (Translated from *Zhurnal Tekh. Fiziki*.)
- [4] J. D. Hoffman and J. J. Weeks, *J. Research NBS* **60**, 465 (1958).
- [5] D. J. Scheiber, *J. Research NBS* **65C** (Eng. and Instr.), 23 (1961).
- [6] T. Nakajima and S. Saito, *J. Poly. Sci.* **31**, 423 (1958).
- [7] J. D. Hoffman, J. J. Weeks, *J. Research NBS*, **66A** (Phys. and Chem.), 13 (1961).
- [8] N. G. McCrum (private communication).
- [9] K. Schmieder and K. Wolf, *Koll. Zeits.* **134**, 149 (1953).
- [10] A. K. Schulz, *J. Chim. Phys.* **53**, 933 (1956).
- [11] K. H. Illers and E. Jenckel, *Koll. Zeits.* **165**, 84 (1959).
- [12] M. L. Williams, R. F. Landel, and J. D. Ferry, *J. Am. Chem. Soc.* **77**, 3701 (1955).
- [13] J. D. Ferry, *Viscoelastic properties of polymers*, J. Wiley & Sons, N.Y., (1961).
- [14] S. Saito and T. Nakajima, *J. Appl. Poly. Sci.* **2**, 93 (1959).
- [15] J. D. Hoffman and J. J. Weeks (manuscript in preparation).
- [16] J. D. Hoffman and J. I. Lauritzen, Jr., *J. Research NBS* **65A** (Phys and Chem.), 297 (1961).
- [17] M. Takayanagi, M. Yoshino, and K. Hoashi, *J. Japan Soc. Testing Materials* **10**, 418 (1961).
- [18] M. Takayanagi, *High polymers, Japan*, **10**, 289 (1961) (In Japanese).
- [19] G. Gee, P. N. Hartley, J. B. M. Herbert, and H. A. Lanceley, *Polymer* **1**, 365 (1960).
- [20] A. B. Thompson and D. W. Woods, *Trans. Faraday Soc.* **52**, 1383 (1956).
- [21] K. S. Cole and R. H. Cole, *J. Chem. Phys.* **9**, 341 (1941).
- [22] J. H. Gladstone and J. Dale, *Phil. Trans.* 153, 317 (1863).
- [23] H. Fröhlich, *Theory of dielectrics*, Oxford Univ. Press, London (1949). See Chapter 2.
- [24] C. I. Carr, Jr., and B. H. Zimm, *J. Chem. Phys.* **18**, 1616 (1950).
- [25] J. D. Hoffman, *J. Chem. Phys.* **20**, 541 (1952).
- [26] J. D. Hoffman and B. F. Decker, *J. Phys. Chem.* **51**, 520 (1953).
- [27] H. S. Kaufman, *J. Am. Chem. Soc.* **75**, 1447 (1953); H. S. Kaufman, *Tech. Assoc. Pulp Paper Ind.* **37**, 140 (1954).
- [28] P. H. Geil (private communication).
- [29] D. H. Reneker (private communication).
- [30] Y. Ishida, Y. Takada, and M. Takayanagi, *Kolloid Zeitschrift* **168**, 121 (1960).
- [31] M. Baccaredda and E. Butta, *J. Poly. Sci.* **44**, 421 (1960).
- [32] K. W. Wagner, *Archiv für Elektrotechnik* **2**, 371 (1914).
- [33] R. W. Sillars, *Inst. of E. E.* **80**, 378 (1937).
- [34] E. A. W. Hoff, D. W. Robinson, and A. H. Willbourn, *J. Poly. Sci.* **18**, 161 (1955).
- [35] K. Deutsch, E. A. W. Hoff, and W. Reddish, *J. Poly. Sci.* **13**, 565 (1954).
- [36] L. Hartshorn and W. H. Ward, *Journal I.E.E.* **79**, 597 (1936).
- [37] E. B. Baker, *Rev. Sci. Instruments* **22**, 379 (1951).
- [38] A.S.T.M. Standards, 1959 Supplement, Part 9, D-150, 7.(a) (1).
- [39] A.S.T.M. Standards, 1959 Supplement, Part 9, D-150, Appendix III.
- [40] W. R. Smythe, *Static and Dynamic Electricity*, 2d ed., ch. 6, McGraw-Hill, 1950.
- [41] I. R. Weingarten, *Annual Report of the Conference on Electrical Insulation*, p. 53, 1955.
- [42] L. Heroux, *J. Appl. Phys.* **29**, 1636 (1958).
- [43] J.V.L. Parry, *Proc. I.E.E.* **98**, 303 (1951).
- [44] C. N. Works, *J. Appl. Phys.* **18**, 605 (1947).
- [45] S. I. Reynolds, *General Electric Review*, Sept. 1947.
- [46] S. Roberts and A. von Hippel, *J. Appl. Phys.* **17**, 610 (1946).
- [47] *Dielectric Materials and Applications*, ed. A. von Hippel, ch. 2, Distributed circuits, William B. Westphal. Published jointly by the Technology Press of MIT, and John Wiley & Sons, Inc., N.Y. (1954).
- [48] P. F. Veselovskii and A. I. Slusker, *Zhur. Tekh. Fiz.* **25**, 939 and 1204, (1955).

(Paper 66A4-162)